JBC RESEARCH ARTICLE

Stabilization of interdomain interactions in G protein α subunits as a determinant of $G\alpha_i$ subtype signaling specificity

Received for publication, October 25, 2023, and in revised form, March 7, 2024 Published, Papers in Press, March 22, 2024,
https://doi.org/10.1016/j.jbc.2024.107211

Tyler J. Lefevre[1,2], Wenyuan Wei[3,‡], Elizaveta Mukhaleva[3,‡], Sai Pranathi Meda Venkata[1], Naincy R. Chandan[1,4], Saji Abraham[1], Yong Li[5], Carmen W. Dessauer[5], Nagarajan Vaidehi[3], and Alan V. Smrcka[1,*]

From the [1]Department of Pharmacology, University of Michigan Medical School, Ann Arbor, Michigan, USA; [2]Program in Chemical Biology, University of Michigan, Ann Arbor, Michigan, USA; [3]Department of Computational and Quantitative Medicine, Beckman Research Institute of the City of Hope, Duarte, California, USA; [4]Genentech, South San Francisco, California, USA; [5]Department of Integrative Biology and Pharmacology McGovern Medical School, UTHealth, Houston, Texas, USA

Reviewed by members of the JBC Editorial Board. Edited by Kirill Martemyanov

Highly homologous members of the $G\alpha_i$ family, $G\alpha_{i1\text{-}3}$, have distinct tissue distributions and physiological functions, yet their biochemical and functional properties are very similar. We recently identified PDZ-RhoGEF (PRG) as a novel $G\alpha_{i1}$ effector that is poorly activated by $G\alpha_{i2}$. In a proteomic proximity labeling screen we observed a strong preference for $G\alpha_{i1}$ relative to $G\alpha_{i2}$ with respect to engagement of a broad range of potential targets. We investigated the mechanistic basis for this selectivity using PRG as a representative target. Substitution of either the helical domain (HD) from $G\alpha_{i1}$ into $G\alpha_{i2}$ or substitution of a single amino acid, A230 in $G\alpha_{i2}$ with the corresponding D in $G\alpha_{i1}$, largely rescues PRG activation and interactions with other potential $G\alpha_i$ targets. Molecular dynamics simulations combined with Bayesian network models revealed that in the GTP bound state, separation at the HD-Ras-like domain (RLD) interface is more pronounced in $G\alpha_{i2}$ than $G\alpha_{i1}$. Mutation of A230 to D in $G\alpha_{i2}$ stabilizes HD-RLD interactions *via* ionic interactions with R145 in the HD which in turn modify the conformation of Switch III. These data support a model where D229 in $G\alpha_{i1}$ interacts with R144 and stabilizes a network of interactions between HD and RLD to promote protein target recognition. The corresponding A230 in $G\alpha_{i2}$ is unable to stabilize this network leading to an overall lower efficacy with respect to target interactions. This study reveals distinct mechanistic properties that could underly differential biological and physiological consequences of activation of $G\alpha_{i1}$ or $G\alpha_{i2}$ by G protein–coupled receptors.

Many physiologically important hormones and neurotransmitters signal through G protein–coupled receptors (GPCRs), rendering these membrane-spanning receptors highly clinically significant as important drug targets (1, 2). GPCRs transduce signals into the cell *via* heterotrimeric G proteins, consisting of the Gα subunit and the Gβγ constitutive heterodimer. Signaling diversity from GPCRs is primarily achieved *via* an array of Gα subunit protein families which harbor distinct downstream signaling capabilities, including the G_s, $G_{i/o}$, $G_{q/11}$, and $G_{12/13}$ families (3–6).

Structurally, Gα subunits consist of a Ras-like domain (RLD), which binds and hydrolyzes guanine nucleotides, and an all-helical domain (HD), connected by a flexible hinge region (5, 7). Much of the investigative focus on Gα protein function has been on the RLD, which harbors three "Switch" regions (Switch I-III) that undergo conformational alterations upon GTP binding. Upon binding GTP, Switch regions I-III collapse toward the bound nucleotide in a conformational rearrangement that permits Gα·GTP-effector interaction after separation from Gβγ and the receptor (8). In contrast, the HD is relatively rigid and opens along the interdomain cleft *via* the flexible hinge in the nucleotide free transition state along the pathway of receptor-mediated GDP release (9–11). Mutation of residues along the Ras-HD interface further increases receptor-independent rate of GDP dissociation in $G\alpha_i$ (12).

Generally, the $G\alpha_s$ family activates adenylyl cyclases (ACs) to produce 3′,5′-cyclic AMP (cAMP) and the $G\alpha_i$ family inhibits ACs (3). The $G\alpha_{i/o}$ family consists of $G\alpha_{i1}$, $G\alpha_{i2}$, $G\alpha_{i3}$, $G\alpha_o$, $G\alpha_{T1}$, $G\alpha_{T2}$, $G\alpha_{T3}$, and $G\alpha_z$. $G\alpha_o$ is prominent in the brain, $G\alpha_T$ in the visual and taste systems, and $G\alpha_z$ in the brain and prostate. $G\alpha_{i2}$ protein expression is more widespread than any other protein in the $G\alpha_{i/o}$ family and it is generally more abundant that $G\alpha_{i1}$ and $G\alpha_{i3}$ (13). $G\alpha_{i2}$ is often expressed alongside $G\alpha_{i3}$ and/or $G\alpha_{i1}$. $G\alpha_{i1\text{-}3}$ subunits are 94% identical between $G\alpha_{i1}$ and $G\alpha_{i3}$, 86% identical between $G\alpha_{i1}$ and $G\alpha_{i2}$, and 88% identical between $G\alpha_{i2}$ and $G\alpha_{i3}$ (14). They have identical rates of single turnover GTP hydrolysis, but the GDP dissociation rate from $G\alpha_{i2}$ is approximately two-fold faster than for the other two isoforms (15).

In terms of signaling specificity, all $G\alpha_i$ subtypes inhibit various AC isoforms with similar potency and efficacy (16). Isoform specific differences have been found in binding to various regulatory proteins including GoLoco/GPR motif containing proteins (17) and regulator of G protein signaling (RGS) proteins (18, 19). Genetic deletion or inactivation of individual $G\alpha_i$ isoforms has yielded evidence for differential function in primary tissues and organisms. For example, KO of $G\alpha_{i2}$ in mice results in exacerbated ischemic injury and cardiac

‡ These authors contributed equally to this work.
* For correspondence: Alan V. Smrcka, avsmrcka@umich.edu.

infarction, while mice lacking Gα$_{i3}$ saw an upregulation in Gα$_{i2}$ and reduced injury (20–24). Additionally, Gα$_{i2}$ primarily promotes arrest, and Gα$_{i3}$ is required for transmigration and chemotaxis in mouse neutrophils (25), while Gα$_{i3}$ activation downstream of CXCR3 has been shown to inhibit Gα$_{i2}$ activation in activated T-cells from mice (26). These data strongly suggest that these isoforms serve non-redundant, unique functions, yet the biochemical features that drive selective functionality is not clearly understood.

Recently, our laboratory used an unbiased proximity interaction screen to identify PDZ-RhoGEF (PRG) as a novel downstream effector of Gα$_i$ (27). Gα$_{i1}$ activates PRG in a nucleotide-dependent and receptor-dependent manner in cells, but Gα$_{i2}$ only weakly stimulates PRG. Here, we interrogated the nature of the specificity of Gα$_i$ subfamily members for PRG activation and found that differences between Gα$_{i1}$ and Gα$_{i2}$ in interactions between the HD and Switch III domains that depend largely on a single amino acid amino difference at position α$^{s4h3.3}$. The weaker interactions between HD and Switch III in Gα$_{i2}$ relative to Gα$_{i1}$ results in weaker PRG engagement by Gα$_{i2}$. Unbiased proximity labeling coupled to tandem mass spectrometry (MS) proteomics supports the idea that this mechanism extends beyond PRG interactions to additional Gα$_i$ targets. Overall, our studies support a model where the strength and frequency of interactions between Gα$_i$ Switch III and the HD control the ability to bind and activate PRG and other targets of Gα$_i$ proteins.

Results

Gα$_{i1}$ more effectively activates and interacts with PRG than Gα$_{i2}$

We have previously shown (27) that Gα$_{i1}$ stimulates PRG and subsequent RhoA activation in a manner dependent on the activation state of Gα$_i$. To mimic the GTP bound state of Gα$_i$, glutamine 204 was substituted with leucine which strongly inhibits GTP hydrolysis leading to constitutive GTP binding and activation (7, 28–30). Transient coexpression of Gα$_{i1}$ Q204L (Gα$_{i1}$ QL), PRG, and a serum responsive element (SRE)-luciferase plasmid that reports on RhoA activation in HEK293 cells (Fig. 1*A*) results in significant PRG activation (Fig. 1*B*). Gα$_{i2}$ Q205L (Gα$_{i2}$ QL) only weakly activates PRG activity in the same assay. Concentration-response experiments show a significant difference in the efficacy of PRG activation by Gα$_{i1}$ QL and Gα$_{i2}$ QL (Fig. 1*C*). This indicates that the difference is not due to differences in GTP binding stoichiometry since this would alter the potency of activation rather than efficacy.

To validate PRG-Gα$_i$ interactions in cells, we performed a NanoBiT nanoluciferase complementation assay (31), in which the NanoLuc LgBiT was inserted after the αA helix in Gα subunits (32), and NanoLuc SmBiT was appended prior to the N-terminal Myc tag of myc-PRG (Fig. 1*D*). Coexpressing Gα$_{i1}$ QL-LgBiT with SmBiT-PRG in HEK293 cells resulted in an increase in luminescent signal relative to Gα$_{i1}$ WT-LgBiT, indicating a nucleotide-dependent interaction with PRG. This was not observed for QL variants in Gα$_{i2}$, Gα$_s$, or Gα$_q$ (Fig. 1*E*). Together, these results show that Gα$_{i1}$ interacts with, and activates PRG in a GTP-dependent manner, while Gα$_{i2}$ is much less efficient in this interaction.

Active Gα$_{i2}$ QL BioID2 weakly engages the proximal interactome relative to Gα$_{i1}$ QL BioID2

Given their previously known functional overlap, the stark disparity between Gα$_{i1}$ and Gα$_{i2}$ in their ability to activate PRG prompted us to probe for further examples of selectivity between Gα$_i$ subtypes. PRG was initially identified as a novel target of Gα$_{i1}$ using unbiased BioID2 proximity labeling coupled to MS. BioID2 functionalizes biotin releasing reactive biotinoyl-5′-AMP, which biotinylates proximal lysines within 20 nm (33). Comparing relative biotinylation by BioID2 fused to either Gα$_i$ WT or Gα$_i$ QL reveals the activated Gα$_i$ proximity interactome. Here, we applied this approach to probe the relative interactomes of Gα$_{i1}$ and Gα$_{i2}$.

Briefly, hemagglutinin tagged (HA)-Gα$_{i1}$ Q204L-BioID2 (Gα$_{i1}$ QL-BioID2), HA-Gα$_{i2}$-BioID2 (Gα$_{i2}$-BioID2), and HA-Gα$_{i2}$ Q205L-BioID2 (Gα$_{i2}$ QL-BioID2) were transiently transfected into HT1080 fibrosarcoma cells and incubated with biotin to allow labeling of proximal proteins by Gα$_i$-BioID2. After 24 h of expression and biotin labeling, cells were lysed, biotinylated proteins were captured with streptavidin beads, and labeled with isobaric tandem mass tag (TMT) labels. Samples from all experimental groups were then analyzed *via* liquid chromatography–tandem MS (LC-MS/MS). Proteins statistically significantly enriched in QL *versus* WT samples are considered proximal interactors. Volcano plots were generated for all the proteins identified with the statistical cutoffs for significance from two different comparisons, Gα$_{i1}$ QL/Gα$_{i2}$ WT (Fig. 2*A* left panel) and Gα$_{i2}$ QL/Gα$_{i2}$ WT (Fig. 2*A* right panel). We assumed that the Gα$_i$ WT interactions would be similar between the two subtypes; thus, Gα$_{i2}$ was used as a baseline for both plots. Validation of this assumption is discussed below.

The identities and fold QL/WT enrichment levels for many hits for active Gα$_{i1}$-BioID2 were consistent with those found in our previous screen (27). Notably, there are no significant observable differences in identity of most of the proteins enriched for interaction with active Gα$_{i1}$ QL-BioID2 *versus* Gα$_{i2}$ QL-BioID2. However, the number of proteins identified that reached statistical significance [-log(abundance ratio *p*-value) ≥ 2.0] were markedly fewer in Gα$_{i2}$ QL-BioID2 samples than in Gα$_{i1}$ QL-BioID2 samples. This is largely because the Gα$_{i2}$ QL-BioID2/Gα$_{i2}$ WT-BioID2 fold enrichment was generally lower than for Gα$_{i1}$ QL BioID2. These data suggest a difference in overall target engagement by Gα$_{i1}$-GTP compared to Gα$_{i2}$-GTP.

To confirm that these observations are not an artifact of the MS analysis and that using Gα$_{i2}$ WT as a baseline in both plots is valid, verification assays were performed with selected "hits" from the MS that showed significant differences between Gα$_{i1}$ QL and Gα$_{i2}$ QL engagement. Epitope-tagged mammalian expression constructs were transiently coexpressed in HEK293 cells with either Gα$_{i1}$-BioID2, Gα$_{i1}$ QL-BioID2, Gα$_{i2}$-

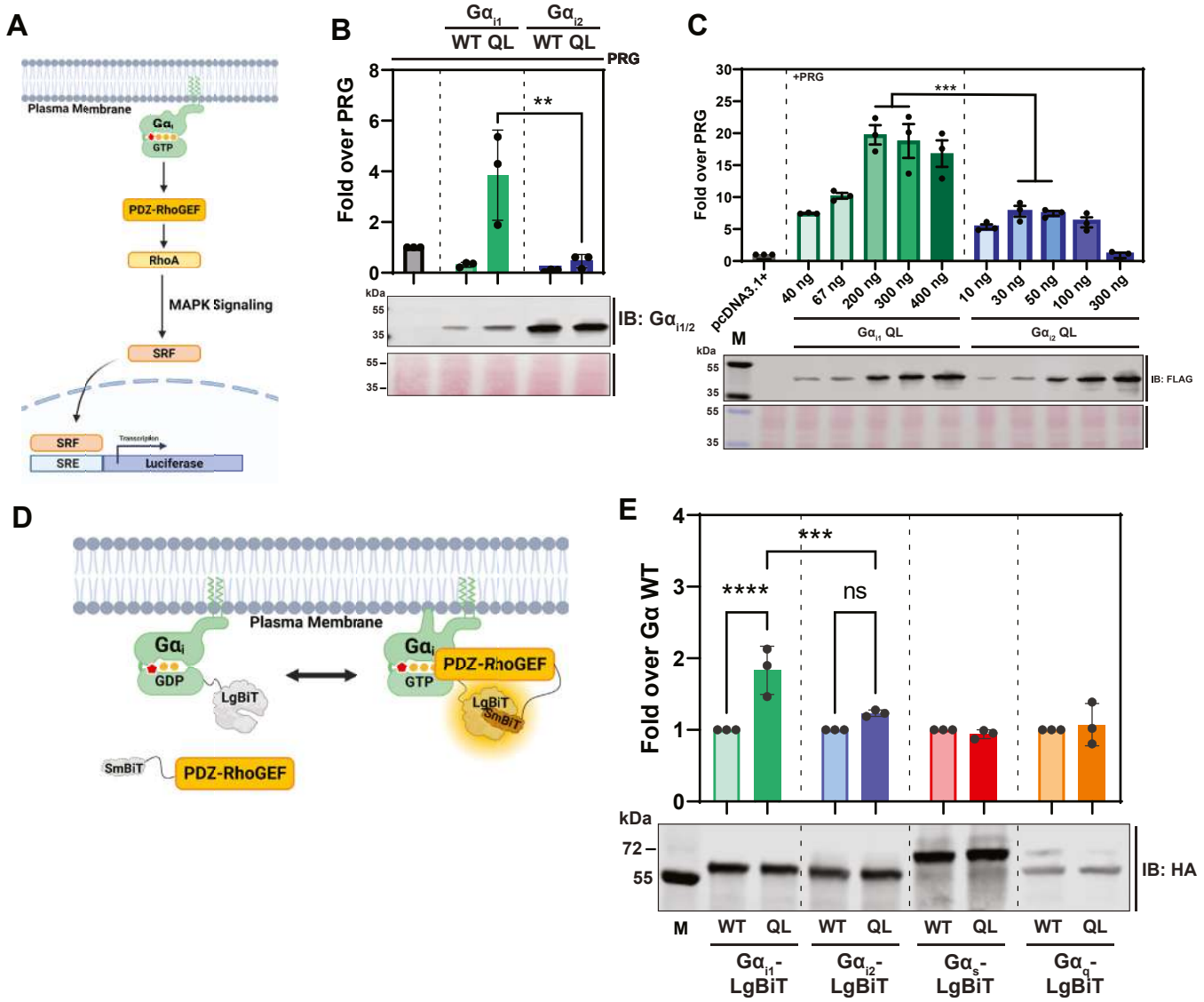

Figure 1. Gα$_{i1}$ more efficiently interacts with PRG than Gα$_{i2}$. *A*, diagram of the SRE luciferase assay used to assess Gα regulation of PRG. HEK293 cells were cotransfected with control plasmid pcDNA 3.1 or Gα plasmids as indicated, PRG, and an SRE luciferase reporter plasmid. Twenty-four hours after transfection One-Glo luciferase reagent was added and luminescence was measured using a plate reader. *B*, comparison of Gα$_{i1}$ and Gα$_{i2}$ which were transfected as indicated. All wells were transfected with PRG. Fold over PRG was calculated as the luminescent signal with Gα subunits co-transfected with PRG divided by the signal with PRG co transfected with control pcDNA 3.1 plasmid. *C*, cells were transfected with the indicated amount of FLAG-Gα$_{i1}$ QL or FLAG-Gα$_{i2}$ QL adjusted to achieve equivalent expression as shown in the flag Western blot shown in the bottom panel. To calculate the significance in the difference in maximal stimulation the values for 200 and 300 ng of Gα$_{i1}$ plasmid were averaged and compared to the average of the 30 and 50 ng values for Gα$_{i2}$. *t* test ***$p < 0.001$. *D*, diagram of the Gα$_i$-LgBiT complementation assay used with Gα$_i$ fused to LgBiT and PRG with N-terminal fusion of SmBiT peptide natural peptide sequence (PRG-SmBiT). *E*, the indicated plasmids were cotransfected into HEK293 cells with PRG-SmBiT. Twenty-four hours after transfection cells were transferred into a 96 well plate and furimazine substrate was added for 15 min prior to measurement of luminescence in a plate reader. All experiments were performed with at least three biological replicates of assays performed in triplicate. Unless otherwise indicated data was analyzed with a one-way ANOVA with a Šídák post test. **$p < 0.01$ and ****$p < 0.0001$. PRG, PDZ-RhoGEF.

BioID2, Gα$_{i2}$ QL-BioID2, or membrane-targeted BioID2 (BioID2-CAAX). Exogenous biotin was added for 24 h, followed by a lysis and streptavidin bead purification. Captured biotinylated protein samples were run on SDS-PAGE and analyzed for pull-down *via* Western blotting using antibodies against the respective affinity tags for the target proteins.

Proteins selected for analysis included several targets that were found in our previous report (27) and represent diverse signaling pathways: PDZ-RhoGEF, α-Parvin (Parvin), vimentin, ribosomal protein S6 kinase A1 (RSK1), neurofibromin 1 (NF1), and Ras p21 protein activator 2 (RASA2). Proteins including NF1, PRG, and Parvin showed selective enrichment in Gα$_{i1}$ QL/WT over Gα$_{i2}$ QL/WT (Figs. 2*B* and S1*D* lanes 3–6). RASA2 showed only a slight preference for interaction with Gα$_{i1}$ QL-BioID2 over Gα$_{i2}$ QL-BioID2, while RSK1 did not preferentially interact with either Gα$_{i1}$ QL-BioID2 or Gα$_{i2}$ QL-BioID2 over the WT-BioID2 variants. These results indicate that many of the proximal interactors found in the proteomic screen are reproducible in an orthogonal assay and are suitable for further analysis in their relationship to Gα$_i$. Importantly, the results confirm that nucleotide-dependent interactions with multiple targets by Gα$_{i2}$ is weaker than for Gα$_{i1}$.

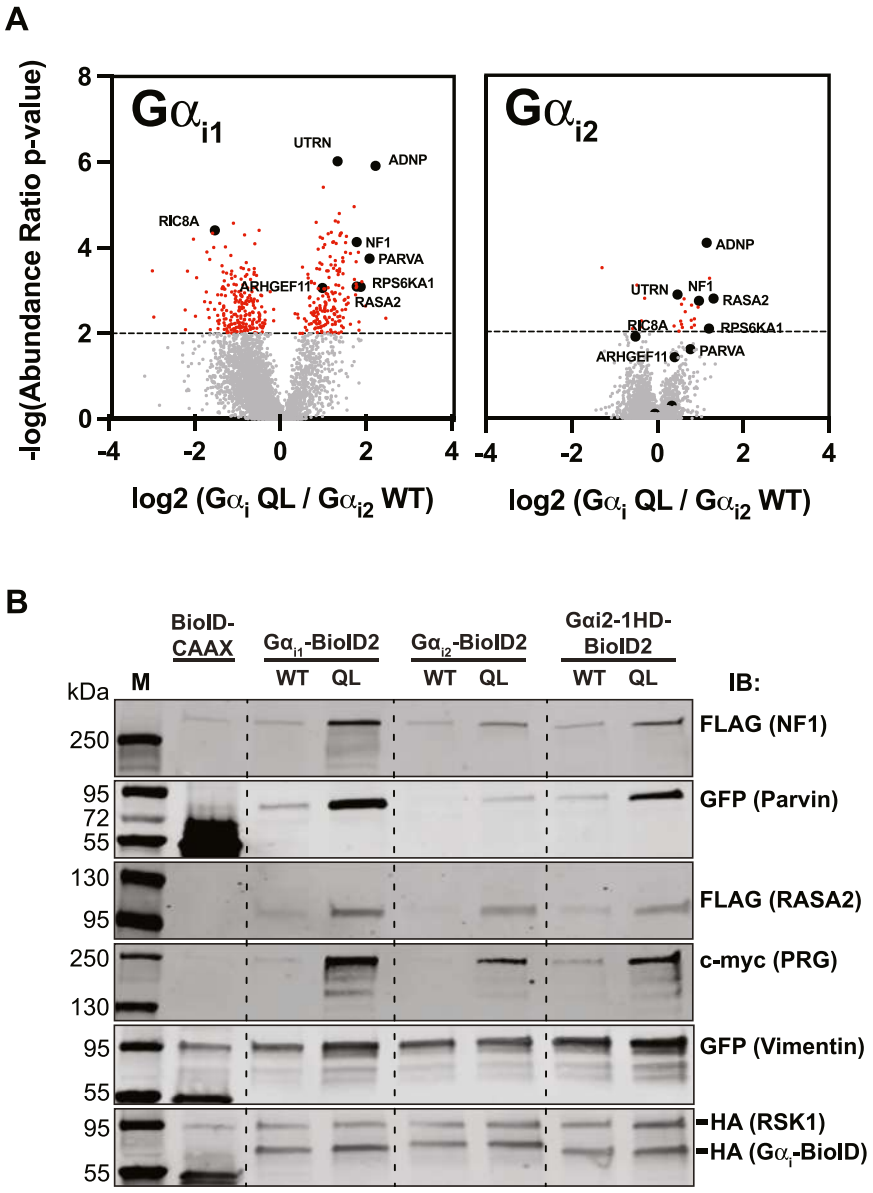

Figure 2. Active Gα$_{i2}$ weakly engages the proximity interactome relative to Gα$_{i1}$. *A*, the indicated HA-Gα$_i$-BioID2 constructs were transiently transfected into HT1080 cells, in triplicate for each condition for 24 h followed by isolation of biotinylated proteins and analysis by TMT mass spectrometry. To control for differences in overall biotinylation each sample was normalized based on the total spectral counts for all of the proteins identified (∼4000 proteins). Spectral counts were then analyzed as the ratio of samples transfected with the Gα$_i$-QL plasmids relative to samples transfected with Gα$_{i2}$ WT. The dashed line indicates a *p* value of 0.01 and all statistically significant proteins are colored in *red*. *B*, the indicated Gα$_i$-BioID2 constructs were cotransfected with the indicated epitope-tagged protein into HEK293 cells. Twenty-four hours after transfection biotinylated proteins were isolated with streptavidin beads and the followed by Western blotting to determine the amount of biotinylated target protein pulled down. Shown is a representative Western blot of an experiment performed twice. TMT, tandem mass tag.

Substitution of the Gα$_{i1}$ HD into Gα$_{i2}$ is sufficient to confer activation of PRG and enhances interactions with other targets

To understand the molecular determinants that drive specificity of activation of PRG by Gα$_{i1}$, and perhaps by extension other targets, we mapped the amino acid differences between the Gα$_i$ subfamily onto a crystal structure of Gα$_{i1}$ bound to a GTP analogue, GPPNHP (Protein Data Bank (PDB) 1CIP). We previously reported that Gα$_{i3}$ activates PRG, so we highlighted amino acids homologous between Gα$_{i1}$ and Gα$_{i3}$ but different from Gα$_{i2}$ (33 residues) (Fig. 3*A*). The HD of Gα$_i$ shows the region of greatest divergence between Gα$_i$ subtypes (Fig. 3, *A* and *B*), containing 21 of the differences between Gα$_{i1}$/Gα$_{i3}$ and Gα$_{i2}$. As an initial approach, we substituted the entire HD of Gα$_{i1}$ (residues 62–167) into the corresponding position in Gα$_{i2}$, resulting in the chimeric Gα$_i$ protein Gα$_{i2}$-1HD (Fig. 3*C*). This chimera is expressed in HEK293 cells and functionally inhibits forskolin-dependent cAMP generation by AC (Fig. S1, *A* and *B*). Gα$_{i2}$-1HD or Gα$_{i2}$-1HD Q205L (QL) were then transfected into HEK293 cells in the SRE-luciferase reporter assay to examine their ability to activate PRG. Strikingly, Gα$_{i2}$-1HD QL expression results in strong activation of PRG as compared to Gα$_{i2}$ QL (Fig. 3*D*), indicating that the HD of

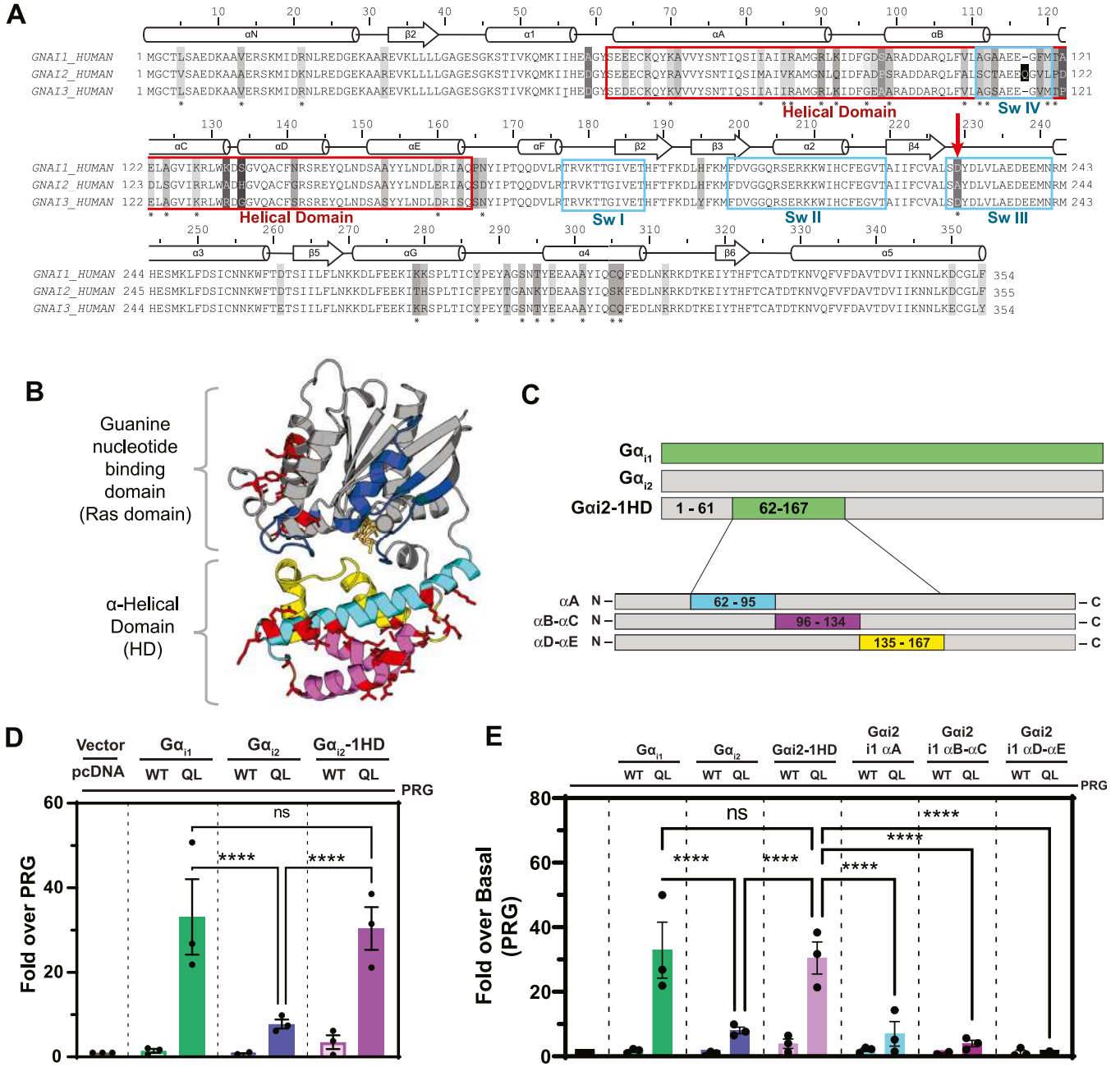

Figure 3. Substitution of the Gα$_{i1}$ helical domain into Gα$_{i2}$ partially restores activation of PRG. *A*, alignment of human Gα$_{i1}$, Gα$_{i2}$, and Gα$_{i3}$. Boxed in *blue* are the Gα$_i$ switch regions. The helical domain is boxed in *red*. Starred (*) amino acids are identical in Gα$_{i1}$ and Gα$_{i3}$ but different in Gα$_{i2}$. *B*, diagrammatic representation of the Gα$_{i1}$ structure. In *cyan*, *magenta*, and *yellow* are subdivisions of the helical domain. Switch I-III are in *blue*. *Red stick* amino acids are amino acids conserved between Gα$_{i1}$ and Gα$_{i3}$ but not Gα$_{i2}$. PDB: 1CIP. *C*, diagram of the constructs used in these experiments. *D*, and *E*, the indicated constructs were cotransfected with PRG and SRE-Luc and the assay was performed as in Figure 1. Western blots for expression and cAMP assays are in Fig. S1 *A–D*. *E*, all SRE-luc experiments were performed with three biological replicates performed in triplicate. Data are ± SEM analyzed by One-way ANOVA with Šídák post-test. ****$p < 0.0001$. PDB, Protein Data Bank; PRG, PDZ-RhoGEF.

Gα$_{i1}$, when substituted into Gα$_{i2}$, is sufficient to confer nucleotide-dependent activation of PRG.

To try to identify structural elements within the Gα$_{i1}$ HD that confer PRG activation, the HD was subdivided into three segments consisting of (1) the Gα αA helix, (2) αB–αC helices, and (3) αD–αE helices. Each of these subdivisions of the Gα$_{i1}$ HD was then substituted into their cognate positions in Gα$_{i2}$ (Fig. 3*C*). Neither the αA helix nor the αB-αC helix subdivisions of Gα$_{i1}$, when substituted into Gα$_{i2}$, activate PRG in cells more than Gα$_{i2}$ Q205L (Fig. 3*E*), but inhibited cAMP generation by AC (Fig. S1*C*). The αD-αE substitution was deficient in the cAMP inhibition assay and could not be analyzed. These data suggest to us that Gα$_{i1}$-mediated activation of PRG relies on some intrinsic property of the intact Gα$_{i1}$ HD rather than one residue or a subset of residues within the Gα$_{i1}$ HD, although we cannot rule out amino acids in the αD and αE helices. It is also possible that the Gα$_{i1}$ HD participates in direct binding interactions with PRG but may also

confer specificity through interactions with some component of the RLD in Gα$_i$.

The striking increase in PRG activation observed with substitution of the Gα$_{i1}$ HD into Gα$_{i2}$ prompted us to test the interaction of these Gα$_{i2}$ variants with other protein targets from the BioID2 proximity labeling screen. We tested multiple targets for activation-dependent labeling using the proximity labeling-dependent Western blotting assay with the WT and QL versions of Gα$_{i1}$, Gα$_{i2}$ and Gα$_{i2}$-1HD (Figs. 2*B* and S1*D* lanes 7, 8). Substitution of the Gα$_{i1}$ HD into Gα$_{i2}$ partially rescues the QL-dependent labeling of some of these targets. Parvin shows the most striking rescue while NF1, PRG, and vimentin show some degree of rescue. RASA2 which does not show a preference for Gα$_{i1}$ *versus* Gα$_{i2}$ is not affected by the HD substitution. These data support the idea that the structural differences conferred by the HD of the Gα$_i$ subunits are important for differences in general target engagement beyond PRG.

Residue A230 in Gα$_{i2}$ controls PRG activation and leads to enhanced proximity interactome engagement

Since we could not identify individual residues in HD that could confer PRG activation we hypothesized that the HD may cooperate with the Ras like domain to confer interactions with PRG. Based on this idea we individually substituted non-conserved residues (amino acids conserved between Gα$_{i1}$ and Gα$_{i3}$ but different in Gα$_{i2}$, starred in Fig. 3*A*) from the Gα$_{i1}$ RLD into Gα$_{i2}$ and determined if they confer activation of PRG. One particular substitution of Gα$_{i2}$ A230$^{s4h3.3}$ with Asp (D229Gα$_{i1}$$^{s4h3.3}$ in Gα$_{i1}$) resulted in enhanced PRG activation (Figs. 4*A* and S2*A*), while the reverse substitution of D229 to Ala in Gα$_{i1}$ blunted PRG activation (Fig. 4*B*). The Gα$_{i2}$ A230D substitution also conferred interactions with PRG in a nucleotide-dependent manner in the NanoBiT complementation assay in (Figs. 4*C* and S2*B*). We chose two of the other targets that show differential Gα$_{i1}$ and Gα$_{i2}$ engagement in the proximity labeling Western blot assay, NF1 and Parvin, and

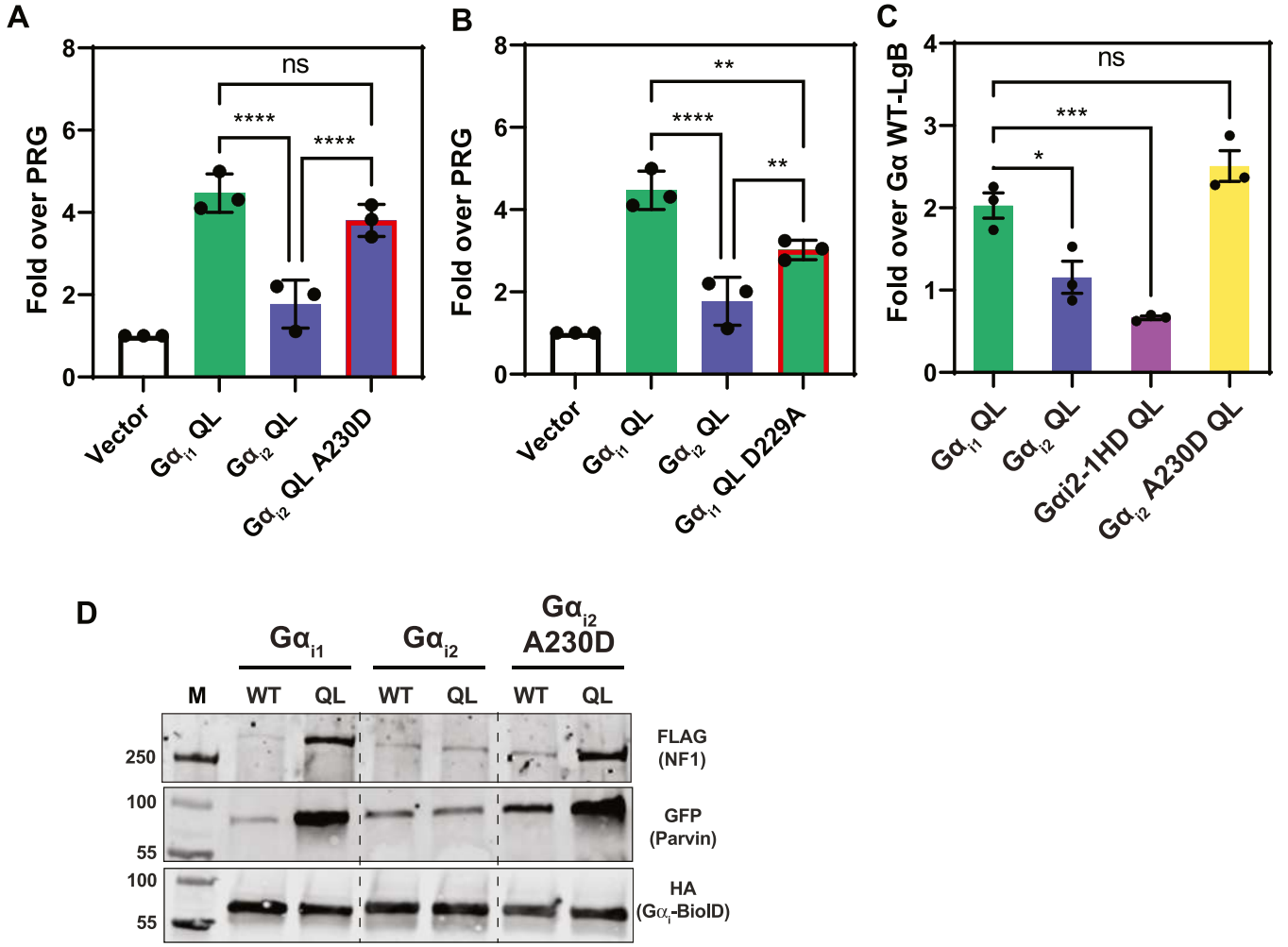

Figure 4. Gα$_{i1}$ D229/Gα$_{i2}$ A230$^{s4h3.3}$ in the Ras-like domain is critical for differences in PRG activation. *A*, mutation of Gα$_{i1}$ D229$^{s4h3.3}$ to the corresponding A in Gα$_{i2}$ (A230$^{s4h3.3}$) reduces the ability to activate PRG. *B*, mutation of Gα$_{i2}$ A230 to the corresponding D in Gα$_{i1}$ (D229) enhances the ability of Gα$_{i2}$ to activate PRG. *C*, mutation of Gα$_{i2}$ A230 to the corresponding D in Gα$_{i1}$ (D229) enhances interactions between Gα$_{i2}$-LgBiT and PRG-SmBiT in the luciferase complementation assay. *D*, mutation of Gα$_{i2}$ A230 to the corresponding *D* in Gα$_{i1}$ (D229) enhances interactions with other proteins in the Gα$_i$ proximity interactome. Shown is representative Western blot for an experiment performed twice. All SRE-luc and complementation experiments were performed with three biological replicates performed in triplicate. Data are ± SEM analyzed by One-way ANOVA with Šídák post test; *$p < 0.05$, **$p < 0.01$, ***$p < 0.001$, ****$p < 0.0001$. PRG, PDZ-RhoGEF.

performed the same assay comparing the QL versions of Gα$_{i1}$-BioID2, Gα$_{i2}$-BioID2 and Gα$_{i2}$ A230D-BioID2 (Figs. 4*D* and S2*C*). The A230D substitution enhances the engagement of Gα$_{i2}$ with these other targets. These data support the idea that the structural differences conferred by either the HD, or A230Gα$_{i2}$/D229Gα$_{i1}$$^{s4h3.3}$, of the Gα$_i$ subunits are important for differences in target engagement beyond PRG. Additionally, the observation that these substitutions restore interactions previously identified in a Gα$_{i1}$ BioID2 proximity labeling screen provides further evidence that these are in fact *bona fide* Gα$_i$ interaction targets that remain to be further characterized physiologically.

Gα$_{i1}$ and Gα$_{i2}$ sample distinct conformations

Examination of the static three-dimensional structure of Gα$_{i1}$ does not clearly indicate why substitution at the D229/A230$^{s4h3.3}$ position, or substitution of the Gα$_{i1}$ HD, would impact binding and/or activation of target proteins. This amino acid is at the base of switchIII near the GTP binding site but is not involved in interactions with the nucleotide, and the closest residue in the HD is 9 Å away (Fig. 5, *A* and *B*). To capture potential interactions that are not observable in the crystal structures, we performed molecular dynamics (MD) simulations with GTP-bound Gα$_{i1}$ and Gα$_{i2}$. We used the crystal structure of Gα$_i$ (PDB ID:1CIP) as a starting structure for Gα$_{i1}$ and generated a homology model of Gα$_{i2}$ using this structure as a template. MD simulations were run for each system totaling to 5 μs. Principal component analysis was used to characterize the dominant motions in Gα$_{i1}$ and Gα$_{i2}$. Principal component 1 (PC1) in both proteins is rotation of the HD and RLD relative to one another (Movies S1 and S3). PC2 is a domain "opening" motion where the HD opens relative to the RLD *via* the interdomain hinge region (Movies S2 and S4). We projected all the snapshots from MD simulations on these two PCs as shown in Figure 5*C*. It is evident from Figure 5*C* (top panel) that Gα$_{i1}$ and Gα$_{i2}$ sample distinct conformation clusters in these PC coordinates. MD simulations show that even when bound to GTP, both Gα$_{i1}$ and Gα$_{i2}$ can explore open and twisted conformations relative to the starting structures and the Gα$_{i2}$ moves farther from its starting conformation more frequently relative to Gα$_{i1}$. When these simulations were done with the A230D substitution in Gα$_{i2}$, a population of conformations moves closer to that of Gα$_{i1}$ (Fig. 5*C* bottom panel). For the mutants Gα$_{i1}$ (D229A) the RLD-HD conformations moved closer to that of Gα$_{i2}$.

To understand the interresidue interactions responsible for the differences in domain interaction dynamics between these G protein subtypes, we analyzed the residues that make the interdomain contacts in all the MD snapshots. We observed differential interactions between residues in Switch III and the αD-αE region of the HD in Gα$_{i1}$ compared to Gα$_{i2}$ (Fig. 5*D*). In Gα$_{i1}$, two key residues in the HD are involved in an interaction network at the HD-RLD interface, Q147$^{hdhe.2}$ and R144$^{HD.11}$. In our simulations during dynamic rotation of the HD-RLD interface, R144$^{HD.11}$ interacts with residues D229$^{s4h3.3}$, D231$^{s4h3.5}$, L232$^{s4h3.6}$, and S228$^{s4h3.2}$ in the Switch III region of the RLD, interactions that are not evident in the crystal structure (Fig. 5*E* left). These interactions are largely absent in Gα$_{i2}$ (Fig. 5*E* mid). In Gα$_{i2}$, substitution of A230 with D partially restores many of the interdomain residue interactions with Switch III that are absent in Gα$_{i2}$ relative to Gα$_{i1}$ (Fig. 5*E* right). Similarly, HD residue Q147$^{hdhe.2}$ is predicted to interact more frequently with A235$^{s4h3.9}$, R242$^{H3.1}$, and V233$^{s4h3.7}$ in Gα$_{i1}$ than the cognate interactions in Gα$_{i2}$. When Gα$_{i2}$ A230$^{s4h3.3}$ is substituted with D, interactions between Q148$^{hdhe.2}$ and V234$^{s4h3.7}$ are strengthened, while other contacts are largely unaffected. This leads to the prediction that Gα$_{i1}$ D229 centers a network of interactions between the HD and RLD-Switch III that are lost in Gα$_{i2}$ (Fig. 5*D*).

To assess the magnitude of domain motions we examined the population distribution of distances between key residues that are involved in the network (Fig. S3). For Gα$_{i1}$ there are two major peaks in the population distribution with ∼50% in a closed conformation centered on 2.5 Å between D229 and R144 and second a broad distribution ranging from 5 to 12 Å (Fig. S3*A*). For Q147-V223 90% of the population distances were centered at 2.5 Å with a small peak at 5 to 7 Å (Fig. S3*B*). This is in strong contrast to Gα$_{i2}$ where 100% A230-R144 distance centered at 10 Å and 90% of Q148-V234 centered at 7.5 Å consistent with a predicted substantially different, more open, conformation at this interface. Substitution of Gα$_{i2}$ A230 with D substantially increases the population at 2.5 Å and decreases the "more open" conformation resulting in distance distributions that more closely resemble that predicted for Gα$_{i1}$. The converse is true for Gα$_{i1}$D229A.

Bayesian network models show that Gα$_{i2}$ A230D mimics Gα$_{i1}$ in RLD-HD interactions

As another approach, a fingerprint matrix of Switch III-HD residue contacts was constructed using data from the simulations. Bayesian Network Analysis was performed on this matrix, yielding a full Bayesian network (shown in Fig. S4 of Supporting Information) that predicts these contacts in Gα$_{i1}$ and Gα$_{i2}$ and their mutants. Each node in this network model represents a predicted residue interaction pair between RLD and HD. Nodes were then ranked by strength to understand their cooperativity ranking within the network. This analysis predicts that interactions between D229$^{s4h3.3}$ in the RLD and R144$^{HD.11}$ in the HD forms the core of a cooperativity network involving multiple contacts in Switch III (Fig. 5*F*, left panel). In the model, this interaction network is disrupted in Gα$_{i2}$ where the D229 cognate residue is alanine (Gα$_{i2}$ A230) which cannot interact with the positively charged arginine (Gα$_{i2}$ R145$^{HD.11}$) (Fig. 5*F*, center panel). Substitution of A230 with D in Gα$_{i2}$ is predicted to restore a cooperative interaction network with Switch III (Fig. 5*F*, right panel). This analysis supports the idea that in GTP-bound Gα$_{i1}$, D229 at the base of Switch III forms an important contact with R144 in the HD that is not observed in crystal structures of Gα$_{i1}$. This interaction supports a network of additional interactions between the HD and multiple amino acids in Switch III that constrain the conformation

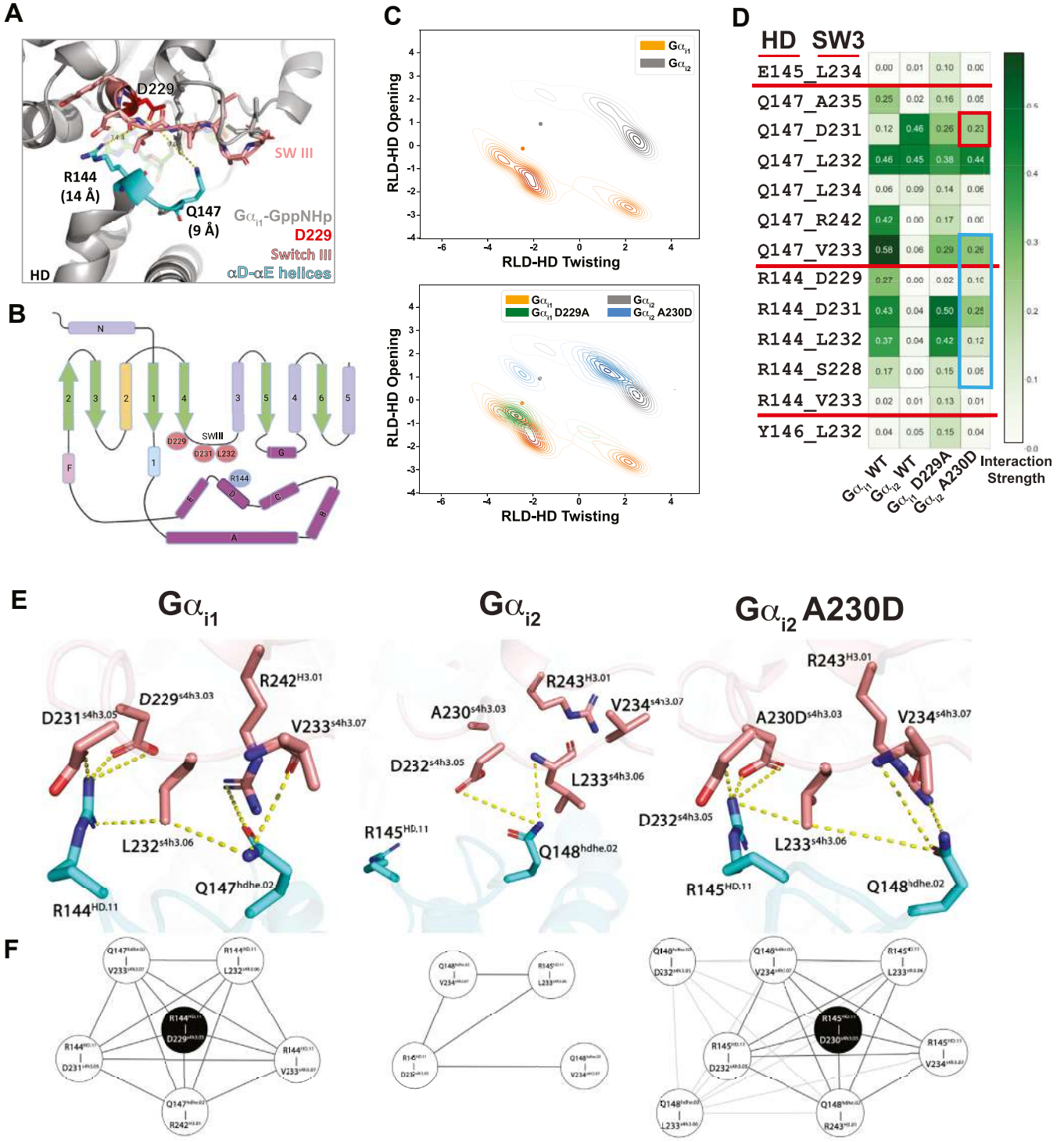

Figure 5. Molecular dynamics simulations and Bayesian network analysis reveal an interaction network that is not apparent in three dimensional crystal structures in the GTP bound state. *A*, diagram of a structure of Gα$_{i1}$-GTP showing the distance between D229 and the nearest HD residues. *B*, ribbon representation of Gα subunit structure highlighting key amino acids at the Switch III-helical domain interface. *C*, principal component analysis of Gα$_{i1}$-GTP *versus* Gα$_{i2}$-GTP. *D*, interaction frequency heat map of amino acid interactions between Switch III amino acids and amino acids in the HD comparing the GTP bound states of Gα$_{i1}$, Gα$_{i2}$, Gα$_{i1}$ D229A, and Gα$_{i2}$ A230D. *E*, diagram of interdomain interactions involving D229 in Gα$_{i1}$-GTP (*top panel*) and A230 in Gα$_{i2}$-GTP (*middle panel*) and Gα$_{i2}$-GTP A230D (*right panel*). *F*, Bayesian networks showing interdomain interactions driven by D229 and HD R144 in Gα$_{i1}$-GTP (*left panel*), in Gα$_{i2}$ A230 cannot interact with R145 weakening the overall interaction network (*middle panel*), Substitution of D for A230 in Gα$_{i2}$-GTP leads to interactions with R145 stabilizing the interaction network between the HD and Switch III. Each node represents a contact made between the HD and Switch III, the thickness of the edge connecting the nodes indicates whether the edge was present in the Gα$_{i1}$ network. HD, helical domain.

of Switch III. This predicted network does not form in Gα$_{i2}$, likely permitting Switch III to adopt conformations other than that seen in Gα$_{i1}$, leading to lower-efficacy interactions with effectors that require Switch III for activation.

PRG stimulation is dependent on interdomain stabilization of Gα$_i$ Switch III

The simulation data indicate that an ionic interaction between D229 in the RLD and R144 in the HD centers an interaction network that controls the conformation of Switch III. Based on this, we predicted that mutation of R144 to disrupt this interaction would reduce PRG activation by Gα$_{i1}$. Gα$_{i1}$ R144A reduces nucleotide-dependent PRG activation in cells, similar to that of Gα$_{i1}$ D229A. When alanine is substituted for both D229 and R144, the same reduction is observed (Figs. 6*A* and S5). Alanine substitution of cognate residue R145 in Gα$_{i2}$ does not alter nucleotide-dependent PRG activation, but completely abolishes activation of PRG conferred by A230D (Figs. 6*B* and S5). These experiments suggest that the D229-R144

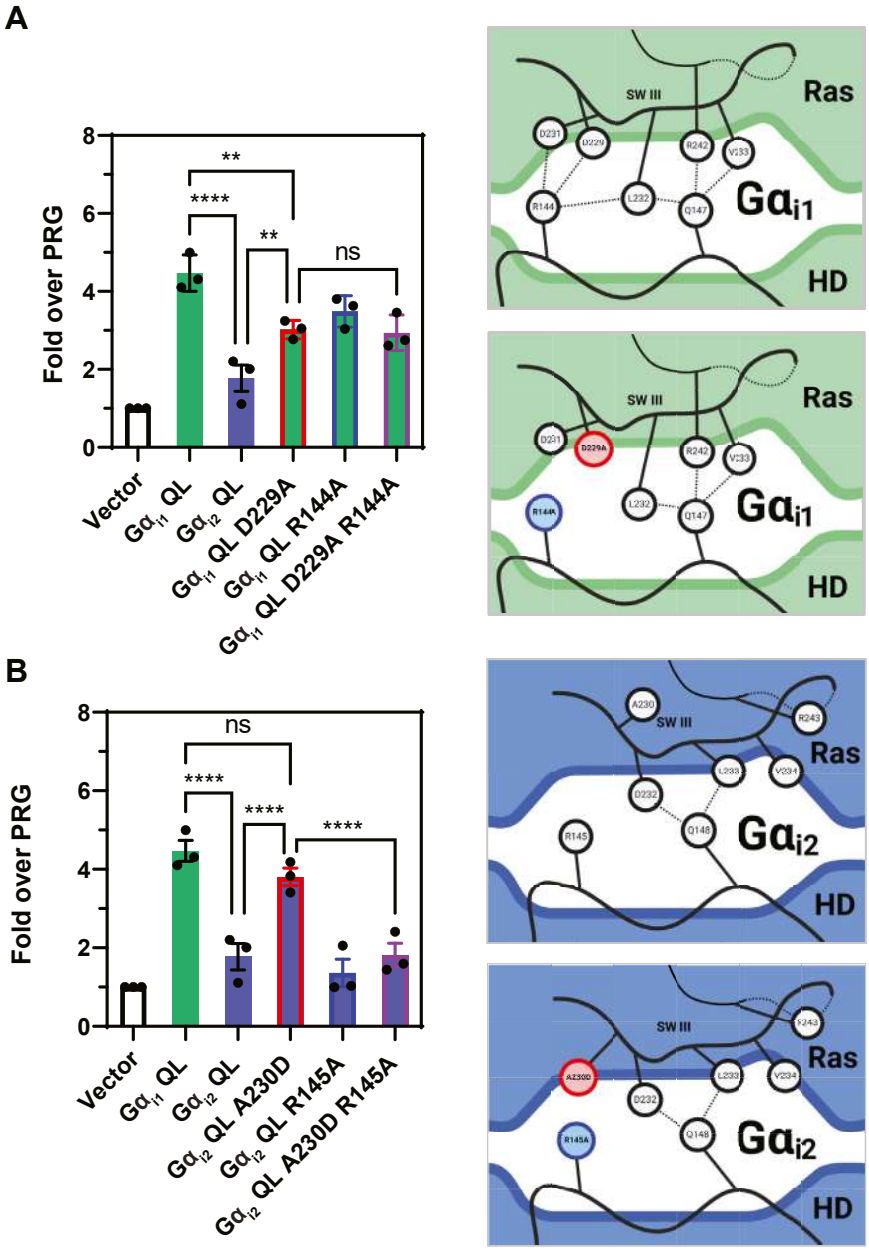

Figure 6. Gα$_{i1}$ D229/Gα$_{i2}$ A230 controls HD-RLD interdomain interactions. *A*, SRE luciferase assay showing PRG activation by QL versions of Gα$_{i1}$, Gα$_{i2}$, Gα$_{i1}$ D229A, Gα$_{i1}$ R144A, and Gα$_{i1}$ D229A-R144A (*left panel*). The *top right panel* is a diagram of the WT Gα$_{i1}$ interaction network. The *bottom right panel* is a diagram of the Gα$_{i1}$ interaction network indicating the amino acid substitutions in *red* and *blue*. *B*, SRE luciferase assay showing PRG activation by QL versions of Gα$_{i1}$, Gα$_{i2}$, Gα$_{i2}$ A230D, Gα$_{i2}$ R145A, and Gα$_{i2}$ A230D-R145A. The *top right panel* is a diagram of the WT Gα$_{i2}$ interaction network. The *bottom right panel* is a diagram of the Gα$_{i2}$ interaction network indicating the amino acid substitutions in *red* and *blue*. Experiments were performed with three biological replicates performed in triplicate. Data are ± SEM analyzed by One-way ANOVA with Šídák post-test; *$p < 0.05$, **$p < 0.01$, ***$p < 0.001$,****$p < 0.0001$. Western blots for protein expression of indicated proteins in A and B are shown in Fig. S5. HD, helical domain; PRG, PDZ-RhoGEF; RLD, Ras-like domain.

interaction contributes to the ability of Gα$_{i1}$ to activate PRG, and the ability to activate PRG conferred to Gα$_{i2}$ by the A230D substitution is entirely dependent on the interdomain D230-R145 interaction.

Switch III is critical for communication to the HD across the domain interface, and affects multiple aspects of Gα protein function, including effector recognition (34, 35) and receptor-mediated activation (36). In the cocrystal structure of Gα$_{13}$ and PRG, Switch III makes multiple contacts with PRG. To test involvement of Switch III in Gα$_i$-dependent PRG activation, we substituted Gα$_{i1}$ Switch III residues D231–A235 (DLVLA) to cognate Gα$_s$ residues N254–R258 (NMVIR) (Gα$_{i1}$ SW3αS). Gα$_{i1}$ SW3αS QL poorly activated PRG compared to Gα$_{i1}$ QL in the SRE luciferase assay (Fig. 7*A*). To confirm that Gα$_{i1}$ SW3αS retains activity, Gα$_{i1}$SW3αS was purified and compared with Gα$_{i1}$ and Gα$_{i2}$ for its ability to inhibit Gα$_s$-stimulated adenylate cyclase. All three proteins were able to equally inhibit AC demonstrating that the Gα$_{i1}$SW3αS chimera is functional (Fig. 7*B*). The loss-of-function mutations in Switch III along with the gain-of-function phenotype achieved by substitution of either Gα$_{i1}$ RLD elements or HD elements provide evidence of cooperation between the RLD and HD stabilizing Switch III in a conformation needed for Gα$_i$-mediated activation of PRG and other targets, but not inhibition of AC (Fig. 7*C*). This network is lost in Gα$_{i2}$.

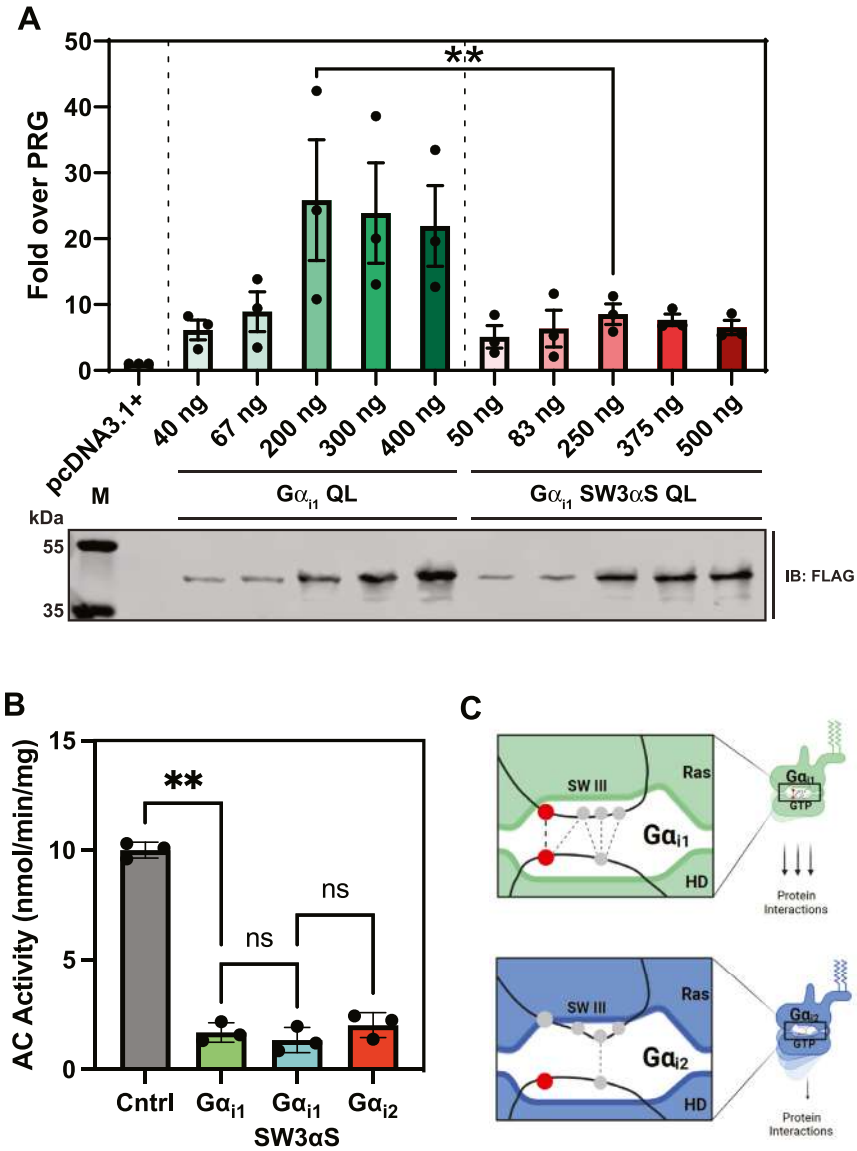

Figure 7. Gα$_{i1}$ Switch III is critical for activation of PRG. *A*, Switch III amino acids in Gα$_{i1}$ were substituted with the cognate amino acids in Gα$_s$ and assayed for PRG activation using the SRE-luc assay. Experiments were performed with three biological replicates performed in duplicate. Data are ± SEM analyzed by One-way ANOVA with Šídák post-test; *$p < 0.05$, **$p < 0.01$, ***$p < 0.001$,****$p < 0.0001$. *B*, structural representation of active Gα$_{i1}$ and active Gα$_{i1}$ with Gα$_s$ substitutions made in Gα$_{i1}$ Switch III. Gα$_{i1}$ is gray, the αD helix in the HD is shown in tan for orientation, Gα$_{i1}$ Switch III residues are shown in *green sticks*, and the Gα$_{i1}$ residues mutated to corresponding residues in Gα$_s$ are in *pink*. PDB ID: 1CIP. *C*, Sf9 membranes expressing hAC6 were assayed in the presence of 10 mM $MgCl_2$, 250 μM ATP, and 30 nM Gα$_s$·GTPγS in the absence and presence of 1 μM myrGα$_{i1}$, myrGα$_{i1}$SW3αS, or myrGα$_{i2}$. mean ± SD, n = 3 performed in duplicate. *D*, overall model of the interactions between the HD and RLD domains of Gα$_i$ subunits that modulate differential interactions between Gα$_i$ subtypes and downstream proteins. HD, helical domain; PDB, Protein Data Bank; PRG, PDZ-RhoGEF; RLD, Ras-like domain.

Discussion

In this study, we provide evidence that Gα$_i$-effector interactions are dependent on the strength and frequency of interaction between Switch III and the HD in the GTP bound state, and that these interactions differ between Gα$_i$ subtypes. The involvement of the Gα$_{i1}$ D229-R144 interaction and other additional interdomain contacts in stabilization of Switch III and effector interactions are supported by multiple key results. First, computational simulations show a dynamic interaction landscape where single substitutions affect the strength of other regional contacts. Second, substitution of either the Gα$_{i1}$ HD or A230D into Gα$_{i2}$ results in increased, GTP-dependent interaction with PRG and other protein targets compared to Gα$_{i2}$ QL. Third, the effects of A230D in the RLD are completely abrogated if R145 in the HD is changed to alanine, strongly supporting the idea that this interdomain linkage is the key to stabilizing the interface. Finally, mutagenesis of Gα$_{i1}$ Switch III eliminates PRG stimulation while retaining the ability to inhibit adenylate cyclase. It is likely that stabilization of Switch III is central to this mechanism because Switch III conformational changes are dependent on the nucleotide binding state (GTP *versus* GDP) while the conformation of the HD is generally not altered upon GTP binding.

While we focused on PRG stimulation as a functional indicator of Gα$_i$ specificity, the Gα$_i$-BioID2 proximity labeling experiments suggest that there are global differences in GTP-dependent interactions between Gα$_i$ subtypes and several novel targets, and that these differences depend on the same substitutions of residues from Gα$_{i1}$ into Gα$_{i2}$ that conferred specificity for PRG activation. A caveat is that proximity methods do not necessarily identify direct binding partners. The proximity labeling-Western blotting assays support the findings from the original screen, but it is possible that GTP-dependence to the labeling of specific proteins is due to GTP dependent interactions with other proteins in larger protein complexes. There is prior data supporting the general finding in a deficiency in Gα$_{i2}$ interactions with some binding partners. One study examined interactions between Gα$_i$ and RGS14 which utilizes a GoLoco/GPR motif to bind to selectively bind to Gα$_i$GDP. It was shown that RGS14 bound to Gα$_{i1}$GDP and Gα$_{i3}$GDP but not Gα$_{i2}$GDP, and this involved amino acids in the HD (17). Another study found that RGS19 (GAIP) binds to Gα$_{i1}$ and Gα$_{i3}$ but not Gα$_{i2}$, and stimulates GTPase activity with the same specificity. Similar to our study, position s4h3.3 (Gα$_{i1}$ D229 and Gα$_{i2}$ A230) was a critical determinant of this difference (19).

All cocrystal structures of Gα subunits with non-RGS effectors show binding to a common cleft between the α2 (Switch II) and α3 helices with no apparent direct involvement of Switch III (37–42). On the other hand, PRG-rgRGS binds to the common effector binding site but also has an N-terminal loop that extends down into the RLD-HD interface, where its conserved IIG motif has contacts between Gα$_{13}$ Switch III, the HD αD-αE loop, and the αA helix (40). This binding mode was also observed between Gα$_{13}$/Gα$_{i1}$ chimera binding to the rgRGS domain of another Dbl-family RhoGEF, P115-RhoGEF (43). Our results and conclusions regarding the influence of Gα$_i$ effector interactions by Switch III stabilization are consistent with the notion that the PRG rgRGS N-terminal segment binds to the domain interface in Gα$_{i1}$. Mutagenic analysis of Gα$_q$-GRK2 interactions revealed involvement of both the HD and Switch III (44), an interaction not evident in the cocrystal structure of Gα$_q$ with GRK2. As another example, Gα$_{T1}$ binding to the autoinhibitory γ subunit of cGMP phosphodiesterase (PDEγ) is dependent on the presence of the HD (45); however, the crystallographic binding site of PDEγ is not in the HD but rather in the α2-α3 cleft (42). Crucially, mutation of a Switch III Glu to Leu abolishes PDE activation by Gα$_T$, with no effects on nucleotide binding or hydrolysis (34). A recent cryo-EM structure of the full cGMP PDE6 αβγ complex with transducin revealed the binding of PDEγ to the outer edge of the Switch III loop as well as the previously solved site in the α2-α3 cleft in Gα$_T$-GTP (46). Thus, there is evidence for involvement of Switch III in effector engagement, and our analysis reveals how two proteins with identical Switch III residues can have differences in target engagement efficacy.

Position s4h3.3 (Gα$_{i1}$ D229 and Gα$_{i2}$ A230) is different for between Gα families but is conserved within each family, except the Gα$_i$ family. Amino acids at this position for each family include Ser in Gα$_s$, Gly in Gα$_o$ and Gα$_z$, Ala in Gα$_T$, and Glu in Gα$_{q/11}$ and Gα$_{12/13}$ (Fig. S6). A similar ionic lock mechanism for stabilization of Switch III through interdomain interactions is likely conserved in the Gα$_{q/11}$ family and Gα$_{13}$, as $R^{HD.11}$ is conserved in these G proteins and could interact in a similar way with $E^{s4h3.3}$ in Switch III. The Gα$_i$ subfamily seems unique in its intrafamily effector specificity achieved by differentiation at s4h3.3 resulting in the presence or absence of the ionic lock.

RLD-HD interactions have classically been understood to be a regulator of nucleotide exchange (12, 47–52), with mutations at the interface intended to disrupt interactions leading to higher rates of GDP dissociation (12). Specifically, mutation of residue R144 in Gα$_{i1}$ to an alanine is known to significantly increase the rate of GTPγS binding, presumably through the breaking of an interdomain interaction with L232 (12). In Gα$_s$, substitution of residues in the Switch III loop to those of Gα$_{i2}$ disrupt the ability of Gα$_s$ to bind GTP in response receptor activation but retains the ability to activate AC in response to GTPγS activation. Activation can then be restored by additionally substituting the Gα$_s$ HD with Gα$_{i2}$ residues (36, 53), demonstrating the importance of Gα isoform-specific interdomain communication for receptor dependent G protein activation.

While it remains untested how lower efficacy of target engagement by Gα$_{i2}$ relative to Gα$_{i1}$ directly leads to distinct physiological roles, our findings are consistent with the notion that Gα$_{i2}$ may in some situations act primarily to regulate AC and act as a scaffold and switch for Gβγ signaling, whereas Gα$_{i1}$ or Gα$_{i3}$ may perform these functions in addition to signaling to various Gα$_i$-specific effectors. This is consistent with known roles for Gα$_{i2}$ and Gα$_{i3}$-mediated signaling events in neutrophils, where Gα$_{i2}$ activation promotes cell arrest

while $G\alpha_{i3}$ promotes migratory phenotypes (25). The effects of activation of $G\alpha_{i2}$ on neutrophil arrest in cells lacking $G\alpha_{i3}$ are similar to those found by Gβγ activation alone (54). The physiological situation is likely to be more complex, and this model cannot fully explain physiological specificity. For example, in murine atria, G protein-gated inwardly rectifying potassium (GIRK) channel activity is differentially regulated by $G\alpha_{i2}$ and $G\alpha_{i1}/G\alpha_{i3}$. Deletion of $G\alpha_{i2}$ increases Gβγ-mediated basal and agonist-induced GIRK currents, while dual KO of $G\alpha_{i1}$ and $G\alpha_{i3}$, which are known to bind and regulate GIRK, ablates basal and muscarinic agonist-induced GIRK activity (55). Nevertheless, it is probable that regulation of interdomain dynamics through the intramolecular interactions we defined play a significant role in physiological specificity.

In conclusion, we describe here a potential mechanism driving effector specificity between $G\alpha_i$ subtypes. In this model switch III is stabilized by an interdomain interaction network with αD-αE residues in the HD, due in part to rearrangement of one nonconserved $G\alpha_i$ Switch III aspartate that contacts a conserved arginine. This stabilization of Switch III not only confers specificity for activation of PDZ-RhoGEF, but appears to be important for interactions with a wider array of targets, shedding light on a possible molecular basis for functional differences in what is generally thought to be functional redundancy in members of the $G\alpha_i$ protein family.

Experimental procedures

Plasmid cDNA constructs

BioID2 fused N terminally with c-Myc tag and C terminally with mVenus, followed by CaaX PM targeting motif (KKKKKKSKTKCVIM, derived from the C terminus of KRas), was a gift from S. Malik of the University of Rochester. C terminally c-Myc–tagged full-length PRG complementary DNA (cDNA) construct in mammalian expression vector was a gift from J. Tesmer of Purdue University. The following plasmids were obtained from Addgene: mEmerald-parvin-C-14 (#54214), EGFP-vimentin-7 (#56439), HA-$G\alpha_i$-BioID2 plasmids in pcDNA3.1+ were constructed as described previously (27).

All Gα clones in pcDNA3.1+ were obtained from the cDNA Resource Center. The sequences of the clones are available upon request.

All mutagenesis to $G\alpha_i$ DNA constructs was accomplished using reagents, protocols, and guidelines from New England Biolabs Q5 Site-Directed Mutagenesis Kit (E0554S). Gαi2-1HD, all $G\alpha_{i1}$ HD subdivision constructs, and $G\alpha_i$ N- and C-terminal substitutions were generated using reagents, protocols, and guidelines from New England Biolabs HiFi DNA Assembly Master Mix (E2621) and Cloning Kit (E5520).

In $G\alpha_{i1}$, a FLAG epitope (DYKDDDDK) was inserted between Ala 121 and Glu 122 and flanked by a flexible linker (SGGGGS) on both sides of the insert. The FLAG epitope in $G\alpha_{i2}$ was inserted in the same manner with the same linkers at the analogous position as $G\alpha_{i1}$, between Asp 122 and Asp 123.

$G\alpha_{i1}$ SW3αS-FLAG was generated using Q5 mutagenesis by substituting $G\alpha_s$ residues N254–R258 (NMVIR) into their cognate position in $G\alpha_{i1}$, D231–A235 (DLVLA) in FLAG-tagged $G\alpha_{i1}$.

SmBiT-PRG was generated by inserting the SmBiT sequence (VTGYRLFEEIL) followed by a flexible linker (SGGGGS) onto the N terminus of cMyc-PRG (cMyc: EQKLISEEDL), resulting in SmBiT-Linker-cMyc-PRG.

Cell culture

A293 and HT1080 cells were obtained from the American Type Culture Collection. A293 and HT1080 cells were grown supplemented in Dulbecco's modified Eagle medium (DMEM) with 10% fetal bovine serum (FBS) (10437028, Gibco) and 100 U of penicillin/streptomycin (15140122, Gibco) at 37 °C with 5% CO2. Trypsin-EDTA (25200056, Gibco) was used for cell passage.

Reagents

The following primary and secondary antibodies were used: $G\alpha_{i1/2}$ (anti-sera) (56), c-Myc (13-2500, Invitrogen), GFP (A11122, Invitrogen), HA (C29F4, Cell Signaling Technology), FLAG (PA1-984B, Invitrogen). Streptavidin-IRDye800 was from LI-COR (925-32230). Primary antibodies were diluted in 3% bovine serum albumin and 0.1% sodium azide and incubated with blots overnight at 4 °C. Streptavidin-IRDye800 was incubated for 1 h at room temperature (RT). For secondary antibodies, goat anti-rabbit DyLight 800 (SA535571, Invitrogen) and goat anti-mouse IRDye 800CW (926-32210, LI-COR) were used at 1:10,000.

NanoBiT luciferase complementation assay

A total of 6.0×10^5 HEK293A cells were seeded in poly-D-lysine coated 6-well plates (Thermo Fisher Scientific FB012927). Immediately after plating, HA-Gα-LgBiT constructs and SmB-cmyc-PDZ-RhoGEF were cotransfected using a 1:3 mass to volume ratio of DNA to Lipofectamine 2000 (Invitrogen). After 24 h, transfection media were aspirated, and cells were gently washed once with 1 ml warm PBS. The PBS was discarded, 200 μl trypsin solution was added, and the plate was incubated at 37 °C and 5% CO_2 for 5 min. Following incubation, 800 μl of warm 1X Hanks' balanced salt solution (HBSS) was added to each well, and the detached cells were aspirated and dispensed into new 15 ml conical tubes. Cells were then pelleted by centrifugation at 250*g* for 5 min at RT. After carefully aspirating the supernatant, each pellet was resuspended in 1 ml warm HBSS, and cell number in each suspension counted. Cell suspensions were centrifuged once more at 250*g* for 5 min at RT and resuspended in warm 10 μM furimazine in HBSS, 1% dimethyl sulfoxide. Subsequently, 5×10^4 cells were distributed to each well in a 96-well plate; samples were analyzed with six technical replicates. The sample plate was incubated at 37 °C for 15 min, followed by a luminescence measurement in each well.

SRE-luciferase reporter assay

96-Well format

A total of 4.5×10^4 HEK293A cells were seeded in poly-D-lysine coated 96-well plates (Greiner Bio-One 655983). Cells were transfected with the following plasmids and amounts per

well: 25 ng SRE-Luc reporter (E134A, Promega), 75 ng $G\alpha_i$ or $G\alpha_i$ QL in pcDNA3.1+, 2.5 ng cmyc-PRG unless otherwise indicated. Minor adjustments in added DNA were made to equalize expression of $G\alpha_i$ subunits based on Western blotting of Flag tagged constructs. In these cases, empty pcDNA3.1+ vector supplemented to equalize total DNA added per well. Transfection took place immediately after seeding with a 1:3 mass to volume ratio of DNA to Lipofectamine 2000 (Invitrogen). Twelve hours after transfection, the media were replaced with 75 µl of serum-free media. Twenty-four hours after transfection, 75 µl (1:1 volume) of One-Glo reagent (E6110, Promega) was added to each well and incubated for 10 min at RT. The luminescence signal was measured using Varioskan LUX multimode microplate reader (Thermo Fisher Scientific).

24-Well format

The SRE-Luc reporter assay was also performed nearly identically in 24-well plates, which offered better well-to-well consistency for technical replicates. 1×10^5 HEK293A cells were seeded in poly-D-lysine coated 24-well plates. One hundred ng SRE-Luc reporter (E134A, Promega), 300 ng $G\alpha_i$ or $G\alpha_i$ QL in pcDNA3.1+, and 5 ng cmyc-PRG DNA were transfected into each well except in $G\alpha_i$ titration experiments, where reduced $G\alpha_i$ DNA was substituted with empty pcDNA3.1+. Transfection took place immediately after seeding with a 1:3 mass to volume ratio of DNA to Lipofectamine 2000 (Invitrogen). Twelve hours after transfection, the media were replaced with 250 µl of serum-free media. Twenty-four hours after transfection, 250 µl (1:1 volume) of One-Glo reagent (E6110, Promega) was added to each well and incubated for 10 min at RT. The luminescence signal was measured using Varioskan LUX multimode microplate reader (Thermo Fisher Scientific). We found that the fold differences in activation by $G\alpha_i$ were lower in the 24-well format but that the technical replicates were more reliable.

GloSensor cAMP assay

A total of 4.5×10^4 HEK293A cells were seeded in poly-D-lysine coated 96-well plates (Greiner Bio-One 655983). Cells were transfected with the following plasmids and amounts per well: 50 ng GloSensor −20F cAMP plasmid (E1171, Promega), 125 ng $G\alpha_i$ or $G\alpha_i$ QL in pcDNA3.1+. In $G\alpha_i$ titration experiments, DNA was supplemented with empty pcDNA3.1+ vector. Transfection took place immediately after seeding with a 1:3 mass to volume ratio of DNA to Lipofectamine 2000 (Invitrogen). Twenty-four hours post transfection, the media were discarded and the cells were loaded with 75 µl 0.5 mg/ml D-Luciferin (L2916, Sigma-Aldrich) in Leibovitz's L-15 medium followed by incubating for 2 h at 37 °C and 5% CO_2. Plates were removed from the incubator and equilibrated at RT. Forskolin was then added to give a 1 mM final concentration and luminescence was measured at 15 min in a plate reader.

Western blotting

Samples in 1X Laemmli sample buffer were resolved on 4 to 20% gradient Mini-PROTEAN TGX gels (4561094, Bio-Rad), transferred to nitrocellulose membranes (Pall 66485), and stained with Ponceau S (141194, Sigma-Aldrich). Membranes were blocked with 3% bovine serum albumin (141194, Sigma-Aldrich) in 0.1% Tween-20 in 20 mM Tris pH 7.5 + 150 mM NaCl (TBST) at RT for 30 min with constant agitation. Primary antibodies were applied for 2 h at RT or overnight at 4 °C. After three RT washes with TBST at 5 min each, secondary antibodies were applied for 1 h. Membranes were imaged on an Odyssey Infrared Imaging System (LI-COR Biosciences).

BioID2 proximity labeling and tandem mass spectrometry analysis

HT1080 cells at passage number up to 15 were used for proximity labeling experiments. Cells were plated into 175 cm^2 flasks at a density of 5.5×10^6 cells per flask. The next day, media were replaced with 35 ml of DMEM containing 50 µM biotin and 10% FBS. Each flask was transfected with 8 µg of plasmid encoding BioID2-fused $G\alpha_i$ construct and 4 µg of YFP cDNA. A total of 0.6 µl of Viromer Red (VR-01LB-00, Lipocalyx) reagent was used per 2 µg of cDNA for transfection, resulting in ∼80 to 85% transfection efficiency. Twenty-four hours after labeling and transfection, the labeling medium were decanted, cells were washed twice with 1× PBS, and harvested at 4000g for 10 min. This step was repeated twice using 1× PBS to recover the maximum number of cells. The supernatant was aspirated, pellets were flash-frozen, and stored at −80 °C until further use.

All stock solutions used for streptavidin pulldown were freshly prepared, except lysis buffer. Low protein binding tubes (022431081, Eppendorf) were used for sample preparation. Frozen pellets were lysed in 1 ml of ice-cold lysis solution (composition described above) for 10 min on ice and incubated with 125 U of benzonase with end over-end rotation at 4 °C for 20 min. A total of 0.3% SDS was added to lysates, which were incubated for another 10 min at 4 °C. Lysates were centrifuged at 15,000*g* for 15 min. The supernatant was transferred to fresh tubes, and the total protein concentration was measured using Pierce 660 nm protein assay reagent. A total of 5% of lysates, adjusted for protein concentration, was reserved to analyze the biotinylation in inputs. The remaining lysates were incubated with 500 µl of Pierce streptavidin magnetic beads slurry per sample in an end-over-end rotator at 4 °C overnight. Beads were washed twice with modRIPA buffer [modRIPA: 50 mM tris, 150 mM NaCl, 0.1% SDS, 0.5% sodium deoxycholate, and 1% Triton X-100 (final pH 7.5)] and once with four different solutions: 1 M KCl, 0.1 M Na_2CO_3, 2% SDS [in 50 mM tris (pH 7.5)], and 2 M urea [in 10 mM tris (pH 8.0)]. Beads were washed twice with 1× PBS and were flash-frozen and stored at −80 °C until further processed for MS.

BioID2 proximity labeling and immunoblot analysis

A total of 1.5×10^6 HEK293A cells were seeded in a poly-D-lysine coated 10 cm plate. The next day, media were replaced with 10 ml DMEM +10% FBS and biotin was added to 50 µM. Cells were transfected with 3 µg of either BioID2-CAAX or one of the $G\alpha_i$-BioID2-HA constructs in pcDNA3.1+, in

addition to 3 μg of one of the effectors of interest (cmyc-PRG, V5-ADNP, RASA2-FLAG, mEmerald-Parvin, RSK1-HA, or GFP-Vimentin). DNA complexes were added to Lipofectamine 2000 solutions with a 1:3 mass:volume ratio (18 μl per plate). After 24 h of expression and labeling, the medium was decanted, cells were rinsed twice with 5 ml of ice cold 1X PBS, scraped off of the plate, and pelleted at 4 °C and 4000g for 10 min. The supernatant was aspirated, and the cell pellets were flash-frozen with liquid N_2 and stored at −80 °C until processed *via* immunoprecipitation.

For the immunoprecipitation, 500 μl ice cold modRIPA was used to resuspend cell pellets. Lysis using benzonase and SDS proceeded as above. Lysates were centrifuged for 15,000*g* for 15 min at 4 °C, and protein concentration was measured using Pierce 660 nm protein assay reagent. After equalizing for protein concentration, 20 μl of each sample volume was retained as an input sample. Five hundred microliters of each equalized sample was added to 170 μl of Pierce streptavidin magnetic bead slurry and rotated end-over-end at 4 °C for at least 2 h to capture biotinylated proteins. Beads were washed three times with ice cold modRIPA and once more with cold 1X PBS. Beads were then resuspended in 100 μl 1X PBS, and 4X Laemmli sample buffer was added to 1X final concentration. Beads were boiled for 10 min at 95 °C, and the supernatant was analyzed by Western blot using anti-HA (1:2000) for $Gα_i$-BioID2-HA and the corresponding antibody for each protein of interest [cmyc-PRG–anti-cmyc (1:2000), V5-ADNP – anti-V5 (1:1000), RASA2-FLAG–anti-FLAG (1:1000), mEmerald-Parvin–anti-GFP (1:1000), RSK1-HA–anti-HA (1:2000), or GFP-Vimentin–anti-GFP (1:1000)].

Protein digestion and TMT labeling

On-bead digestion followed by LC-MS/MS analysis was performed at the MS-based Proteomics Resource Facility of the Department of Pathology at the University of Michigan. Samples were reduced (10 mM DTT in 0.1 M triethylammonium bicarbonate at 45 °C for 30 min), alkylated (55 mM 2-chloroacetamide at RT for 30 min in the dark), and subsequently digested using a 1:25 ratio of trypsin (V5113, Promega):protein at 37 °C with constant mixing. A total of 0.2% TFA was added to stop the proteolysis, and peptides were desalted using a Sep-Pak C18 cartridge (WAT036945, Waters Corp). The desalted peptides were dried in a vacufuge and reconstituted in 100 μl of 0.1 M triethylammonium bicarbonate. A TMT10plex Isobaric Label Reagent Set plus TMT11 to 131C Label Reagent kit (A37725, Thermo Fisher Scientific) was used to label each sample per the manufacturer's protocol. The samples were labeled with TMT 11-plex reagents at RT for 1 h. The reaction was quenched by adding 8 μl of 5% hydroxylamine for 15 min and dried. An offline fractionation of the combined sample into eight fractions was performed using a high pH reverse-phase peptide fractionation kit, as per the manufacturer's protocol (84868, Pierce). Fractions were dried and reconstituted in 12 μl of 0.1% formic acid/2% acetonitrile for LC-MS/MS analysis.

LC-MS analysis

An Orbitrap Fusion (Thermo Fisher Scientific) and RSLC Ultimate 3000 nano-UPLC (Dionex) were used to acquire the data. For superior quantitation accuracy, we used multinotch-MS3 (57). Two microliters of each fraction was resolved on a nanocapillary reverse-phase column (75 μm internal diameter by 50 cm; PepMap RSLC C18 column, Thermo Fisher Scientific) at a flow rate of 300 nl/min using 0.1% formic acid/acetonitrile gradient system (2–22% acetonitrile in 110 min; 22–40% acetonitrile in 25 min; 6-min wash at 90% acetonitrile; and 25 min reequilibration) and directly sprayed onto the Orbitrap Fusion using EasySpray source (Thermo Fisher Scientific). The mass spectrometer was set to collect one MS1 scan [Orbitrap; 120,000 resolution; automatic gain control (AGC) target 2 × 105; max IT (maximum ionization time) 50 ms] and data-dependent, "Top Speed" (3 s) MS2 scans [collision-induced dissociation; ion trap; normalized collision energy 35; AGC 5 × 103; max IT 100 ms]. For multinotch-MS3, the top 10 precursors from each MS2 were fragmented by high energy collisional dissociation, followed by Orbitrap analysis (normalized collision energy 55; 60,000 resolution; AGC 5 × 104; max IT 120 ms, 100–500 mass/charge ratio scan range).

Purification of $Gα_i$ subunits

C terminally hexahistidine tagged $Gα_i$ subunits and chimeras were coexpressed with *N*-myristoyltransferase in *Escherichia coli* as previously described (58). Proteins were purified using Ni-NTA chromatography using a gradient from 0 to 200 mM imidazole which resulted in proteins of greater than 90% purity. Myristoylation was confirmed by analyzing molecular weights on SDS-PAGE and G protein nucleotide binding activity was assessed using [^{35}S]-GTPγS binding. All proteins had 20 to 40% nucleotide binding activity.

Adenylyl cyclase activity assays

Membranes from Sf9 cells expressing hAC6 (10 μg per reaction) were assayed for AC activity as described (59). Purified and GTPγS-activated myristoylated $Gα_{i1}$SW3αs, $Gα_{i1}$ and $Gα_{i2}$ were preincubated with membranes for 5 min on ice. $Gα_s$·GTPγS (30 nM final) was added and preincubated for 5 min on ice prior to the start of the assay (10 min at 30 C). Reactions were stopped with 0.2 N HCl, and cAMP was detected by enzyme immunoassay (Assay Designs).

Generating structural models and MD simulations

The structural model of monomeric GTP-bound $Gα_{i1}$ and $Gα_{i2}$ protein with Mg^{2+} ion was built using the monomeric GTP bound rat $Gα_{i1}$ crystal structure (PDB ID: 1CIP) as template and using the homology modeling method in the Prime module of Maestro software from Schrodinger (https://www.schrodinger.com/products/maestro). The GNP present in the original crystal structure was converted to GTP using Maestro edit panel. Point mutations to generate the structures of $Gα_{i1}^{D229A}$ and $Gα_{i2}^{A230D}$ were performed using Maestro Biologics suite. The side chain packing was done for all the

residues within 5 Å of the mutated residue position including the mutated residues using Maestro Prime suite. All structures further underwent energy minimization using conjugate gradient method with a convergence cutoff of 0.1 kcal/mol/Å. Input files for MD simulations were generated using CHARMM-GUI (60). Each monomeric $G\alpha_i$ protein was solvated in explicit TIP3P water molecules in a cubic box (9.0 nm × 9.0 nm × 9.0 nm) with 0.15 M of potassium chloride to mimic the physiological condition. We used GROMACS software (61) (Version 2021.3) (https://www.gromacs.org) with all-atom CHARMM36 force field (62) to perform MD simulations. MD simulations were performed at 310°K coupled to a temperature bath with a relaxation time of 0.1 ps (63). Pressure of the systems was calculated with molecular virial and was held constant by a weak coupling to a pressure bath with a relaxation time of 0.5 ps. Equilibrium bond length and geometry of water molecules were constrained using the SHAKE algorithm (64). The short-range electrostatic and van der Waals interactions were estimated every 2 fs using a charged group pair list with cutoff of 8 Å between centers of geometry of charged groups. Long-range van der Waals interactions were calculated using a cutoff of 14 Å and long-range electrostatic interactions were treated with the particle mesh Ewald method (65). Temperature was kept constant at 310°K by applying the Nose–Hoover thermostat (66). Desired pressure for all systems were achieved by using Parrinello–Rahman barostat with a pressure relaxation time of 2 ps (67). Before production runs, all systems were subjected to a 5000-step steepest descent energy minimization to remove bad contacts (68). After minimization, the systems were heated up to 310°K under constant temperature-volume ensemble (NVT). The simulations were saved every 200 ps for analysis. The protein, Mg^{2+} ion, and nucleotide were subjected to positional constraints under a harmonic force constant of 1000 kJ/(mol*nm^2) during the NVT step while solvent molecules were free to move. The systems then were further equilibrated using a constant pressure ensemble (NPT), in which the force constant is applied to the protein, Mg^{2+} ion, and nucleotide were gradually reduced from 5 kJ/(mol*nm^2) to zero in six steps of 5 ns each. An additional 50 ns of unconstraint simulation was performed, making it a total of 80 ns NPT equilibration prior to production runs. We performed five production runs of 1000 ns each using five different initial velocities for every system. Therefore, we had 5 μs long MD trajectories for both WT and mutant systems of $G\alpha_{i1}$ and $G\alpha_{i2}$ protein.

Principal component analysis and representative structures

The last 600 ns of five independent MD simulation runs were merged into one concatenated trajectory for each system. Two merged trajectories were further created based on the concatenated trajectories: one contains the WT $G\alpha_{i1}$ and $G\alpha_{i2}$ trajectories, and the other contains all four trajectories. PC analysis was performed on each merged trajectory using the gmx covar module of GROMACS with covariance matrix of C alpha atoms of all residues. The first two principal components (PC1 and PC2) of every system were extracted using gmx anaeig module of GROMACS and imported into Python as a data-frame using the Pandas package. Kernel density estimation maps were generated using Python Seaborn package (version 0.9.0) (https://seaborn.pydata.org) and plotted using Python Matplotlib package (https://matplotlib.org).

Representative structure extraction

Using Get-contact data (see Calculating the fingerprints of pairwise interactions between HD and switch III domain of G protein), frame numbers in $G\alpha_{i2}^{A230D}$ trajectory that have contacts between R145 and D230 were recorded. The corresponding frames were extracted from the trajectory using gmx trjconv module of GROMACS. The representative structure of $G\alpha_{i1}$ was used as template, and the RMSD values of the extracted $G\alpha_{i2}^{A230D}$ frames were calculated using gmx rms module: C alpha atoms were selected for both alignment and calculation. The frame with the smallest RMSD value was selected as the representative structure for $G\alpha_{i2}^{A230D}$ system.

Calculating the fingerprints of pairwise interactions between HD and switch III domain of G protein

The analysis of the landscape of pairwise intermolecular residue contacts between the HD domain and switch III region of $G\alpha_i$ with MD simulations using the "getcontacts" python script library (https://www.github.com/getcontacts). This was utilized to identify various types of contacts, including salt-bridges (<4.0 Å cutoff between anion and cation atoms), hydrogen bonds (<3.5 Å cutoff between hydrogen donor and acceptor atoms, <70° angle between donor and acceptor), van der Waals (<2 Å difference between two atoms), pi-stack contacts (<7.0 Å distance between aromatic centers of aromatic residues, <30° angle between normal vectors emanating from aromatic plane of each residue), and cation-pi contacts (<6.0 Å distance between cation atom and centroid of aromatic rink, <60° angle between normal vector from aromatic plane to cation atom). To conduct the analysis, the MD simulation trajectories were concatenated into 1 μs ensembles and stored as xtc coordinate files. Subsequently, water and ions were stripped from the trajectory files utilized for the contact analysis, and atom selection groups were matched with the relevant amino acid residues for each protein domain. In-house python scripts were used to perform one-hot encoding to generate a binary fingerprint for each simulation. The one-hot encoding represented the presence of a contact between two residues in a particular frame with "1" and its absence with "0".

Bayesian network analysis

Binary fingerprints of residue contact pairs were analyzed to understand their interdependent interactions using BNOmics, software developed for Bayesian network analysis (https://bitbucket.org/77D/bnomics). Separate Bayesian networks were first constructed for each G protein type. Heuristic network model selection search (69) was carried out with 50 random restarts, to ensure convergence. Bayesian networks of contact fingerprints have residue pairs as nodes and the edge weight between the nodes correlates with the dependency between them. As a measure of contact pairs' connectivity, the

network property of node strength was used—the total sum of edge weights belonging to this node. After sorting the residue pairs from highest node strength to the lowest, the top 25 percentile of them was compared between different G protein types. Graphical representation of these nodes and their interconnections were demonstrated using network visualization software Cytoscape 3.9.1 (https://cytoscape.org/).

Data availability

The MS proteomics data has been deposited to the ProteomeXchange Consortium *via* the PRIDE partner repository. All other data needed to evaluate the conclusions in the manuscript are present in the manuscript.

Supporting information—This article contains supporting information.

Author contributions—T. J. L., W. W., E. M., S. P. M. V., S. A., and Y. L. investigation; T. J. L., W. W., E. M., N. R. C., C. W. D., N. V., and A. V. S. conceptualization; T. J. L., W. W., E. M., and A. V. S. formal analysis; T. J. L. writing–original draft; W. W., E. M., C. W. D., N. V., and A. V. S. writing–review and editing; N. R. C. and A. V. S. methodology; C. W. D., N. V., and A. V. S. funding acquisition; A. V. S. validation; A. V. S. resources; A. V. S. data curation; A. V. S. supervision.

Funding and additional information—This work was supported by National Institutes of Health Grants R35GM127303 (to A. V. S), and AHA 826816 (to T. J. L.), and R01-GM117923 and R01-LM013876 (to N. V.). The content is solely the responsibility of the authors and does not necessarily represent the official views of the National Institutes of Health.

Conflict of interest—The authors declare that they have no conflicts of interest with the contents of this article.

Abbreviations—The abbreviations used are: AC, adenylyl cyclase; AGC, automatic gain control; cDNA, complementary DNA; DMEM, Dulbecco's modified Eagle medium; FBS, fetal bovine serum; GPCR, G protein–coupled receptor; HBSS, Hanks' balanced salt solution; HD, helical domain; LC-MS/MS, liquid chromatography–tandem MS; MD, molecular dynamics; MS, mass spectrometry; NF1, neurofibromin 1; PC, principal component; PDB, Protein Data Bank; PDE, phosphodiesterase; PRG, PDZ-RhoGEF; RASA2, Ras p21 protein activator 2; RLD, Ras-like domain; RSK1, ribosomal protein S6 kinase A1; RT, room temperature; TMT, tandem mass tag.

References

1. Sriram, K., and Insel, P. A. (2018) G protein-coupled receptors as targets for Approved drugs: how many targets and how many drugs? *Mol. Pharmacol.* **93**, 251–258
2. Hauser, A. S., Attwood, M. M., Rask-Andersen, M., Schioth, H. B., and Gloriam, D. E. (2017) Trends in GPCR drug discovery: new agents, targets and indications. *Nat. Rev. Drug Discov.* **16**, 829–842
3. Gilman, A. G. (1987) G proteins: transducers of receptor-generated signals. *Annu. Rev. Biochem.* **56**, 615–649
4. Hepler, J. R., and Gilman, A. G. (1992) G proteins. *Trends Biochem. Sci.* **17**, 383–387
5. Oldham, W. M., and Hamm, H. E. (2008) Heterotrimeric G protein activation by G-protein-coupled receptors. *Nat. Rev. Mol. Cell Biol.* **9**, 60–71
6. Calebiro, D., Koszegi, Z., Lanoiselee, Y., Miljus, T., and O'Brien, S. G. (2021) protein-coupled receptor-G protein interactions: a single-molecule perspective. *Physiol. Rev.* **101**, 857–906
7. Coleman, D. E., Berghuis, A. M., Lee, E., Linder, M. E., Gilman, A. G., and Sprang, S. R. (1994) Structures of active conformations of Gi alpha 1and the mechanism of GTP hydrolysis. *Science* **265**, 1405–1412
8. Knight, K. M., Ghosh, S., Campbell, S. L., Lefevre, T. J., Olsen, R. H. J., Smrcka, A. V., *et al.* (2021) A universal allosteric mechanism for G protein activation. *Mol. Cell* **81**, 1384–1396.e6
9. Van Eps, N., Preininger, A. M., Alexander, N., Kaya, A. I., Meier, S., Meiler, J., *et al.* (2011) Interaction of a G protein with an activated receptor opens the interdomain interface in the alpha subunit. *Proc. Natl. Acad. Sci. U. S. A.* **108**, 9420–9424
10. Chung, K. Y., Rasmussen, S. G. F., Liu, T., Li, S., DeVree, B. T., Chae, P. S., *et al.* (2011) Conformational changes in the G protein Gs induced by the β2 adrenergic receptor. *Nature* **477**, 611–615
11. Rasmussen, S. G. F., DeVree, B. T., Zou, Y., Kruse, A. C., Chung, K. Y., Kobilka, T. S., *et al.* (2011) Crystal structure of the β2 adrenergic receptor–Gs protein complex. *Nature* **477**, 549–555
12. Remmers, A. E., Engel, C., Liu, M., and Neubig, R. R. (1999) Interdomain interactions regulate GDP release from heterotrimeric G proteins. *Biochemistry* **38**, 13795–13800
13. Wang, D., Eraslan, B., Wieland, T., Hallström, B., Hopf, T., Zolg, D. P., *et al.* (2019) A deep proteome and transcriptome abundance atlas of 29 healthy human tissues. *Mol. Syst. Biol.* **15**, e8503
14. Itoh, H., Toyama, R., Kozasa, T., Tsukamoto, T., Matsuoka, M., and Kaziro, Y. (1988) Presence of three distinct molecular species of Gi protein alpha subunit. Structure of rat cDNAs and human genomic DNAs. *J. Biol. Chem.* **263**, 6656–6664
15. Linder, M. E., Ewald, D. A., Miller, R. J., and Gilman, A. G. (1990) Purification and characterization of Go alpha and three types of Gi alpha after expression in Escherichia coli. *J. Biol. Chem.* **265**, 8243–8251
16. Taussig, R., Tang, W. J., Hepler, J. R., and Gilman, A. G. (1994) Distinct patterns of bidirectional regulation of mammalian adenylyl cyclases. *J. Biol. Chem.* **269**, 6093–6100
17. Mittal, V., and Linder, M. E. (2004) The RGS14 GoLoco domain discriminates among Galphai isoforms. *J. Biol. Chem.* **279**, 46772–46778
18. Hooks, S. B., Waldo, G. L., Corbitt, J., Bodor, E. T., Krumins, A. M., and Harden, T. K. (2003) RGS6, RGS7, RGS9, and RGS11 stimulate GTPase activity of Gi family G-proteins with differential selectivity and maximal activity. *J. Biol. Chem.* **278**, 10087–10093
19. Woulfe, D. S., and Stadel, J. M. (1999) Structural basis for the selectivity of the RGS protein, GAIP, for Galphai family members. Identification of a single amino acid determinant for selective interaction of Galphai subunits with GAIP. *J. Biol. Chem.* **274**, 17718–17724
20. Köhler, D., Devanathan, V., Bernardo de Oliveira Franz, C., Eldh, T., Novakovic, A., Roth, J. M., *et al.* (2014) Gαi2- and Gαi3-deficient mice Display Opposite Severity of Myocardial ischemia Reperfusion injury. *PLoS One* **9**, e98325
21. DeGeorge, B. R., Jr., Gao, E., Boucher, M., Vinge, L. E., Martini, J. S., Raake, P. W., *et al.* (2008) Targeted inhibition of cardiomyocyte Gi signaling enhances susceptibility to apoptotic cell death in response to ischemic stress. *Circulation* **117**, 1378–1387
22. Dizayee, S., Kaestner, S., Kuck, F., Hein, P., Klein, C., Piekorz, R. P., *et al.* (2011) Galphai2- and Galphai3-specific regulation of voltage-dependent L-type calcium channels in cardiomyocytes. *PLoS One* **6**, e24979
23. Foerster, K., Groner, F., Matthes, J., Koch, W. J., Birnbaumer, L., and Herzig, S. (2003) Cardioprotection specific for the G protein Gαi2 in chronic adrenergic signaling through β2-adrenoceptors. *Proc. Natl. Acad. Sci. U. S. A.* **100**, 14475–14480
24. Kaur, K., Parra, S., Chen, R., Charbeneau, R. A., Wade, S. M., Jay, P. Y., *et al.* (2012) Gαi2 signaling: friend or foe in cardiac injury and heart failure? *Naunyn Schmiedebergs Arch. Pharmacol.* **385**, 443–453
25. Kuwano, Y., Adler, M., Zhang, H., Groisman, A., and Ley, K. (2016) Gαi2 and Gαi3 differentially regulate arrest from Flow and chemotaxis in mouse neutrophils. *J. Immunol.* **196**, 3828–3833

26. Thompson, B. D., Jin, Y., Wu, K. H., Colvin, R. A., Luster, A. D., Birnbaumer, L., *et al.* (2007) Inhibition of Gαi2 activation by Gαi3 in CXCR3-mediated signaling. *J. Biol. Chem.* **282**, 9547–9555
27. Chandan, N. R., Abraham, S., SenGupta, S., Parent, C. A., and Smrcka, A. V. (2022) A network of Gαi signaling partners is revealed by proximity labeling proteomics analysis and includes PDZ-RhoGEF. *Sci. Signal.* **15**, eabi9869
28. Masters, S. B., Miller, R. T., Chi, M. H., Chang, F. H., Beiderman, B., Lopez, N. G., *et al.* (1989) Mutations in the GTP-binding site of GSα alter stimulation of adenylyl cyclase. *J. Biol. Chem.* **264**, 15467–15474
29. Graziano, M. P., and Gilman, A. G. (1989) Synthesis in Escherichia coli of GTPase-deficient mutants of Gsα. *J. Biol. Chem.* **264**, 15475–15482
30. Wong, Y. H., Federman, A., Pace, A. M., Zachary, I., Evans, T., Pouysségur, J., *et al.* (1991) Mutant α subunits of Gi2 inhibit cyclic AMP accumulation. *Nature* **351**, 63–65
31. Dixon, A. S., Schwinn, M. K., Hall, M. P., Zimmerman, K., Otto, P., Lubben, T. H., *et al.* (2016) NanoLuc complementation reporter Optimized for accurate measurement of protein interactions in cells. *ACS Chem. Biol.* **11**, 400–408
32. Laschet, C., Dupuis, N., and Hanson, J. (2019) A dynamic and screening-compatible nanoluciferase-based complementation assay enables profiling of individual GPCR-G protein interactions. *J. Biol. Chem.* **294**, 4079–4090
33. Kim, D. I., Jensen, S. C., Noble, K. A., Kc, B., Roux, K. H., Motamedchaboki, K., *et al.* (2016) An improved smaller biotin ligase for BioID proximity labeling. *Mol. Biol. Cell* **27**, 1188–1196
34. Li, Q., and Cerione, R. A. (1997) Communication between switch II and switch III of the transducin α subunit is Essential for target activation. *J. Biol. Chem.* **272**, 21673–21676
35. Pereira, R., and Cerione, R. A. (2005) A switch 3 Point mutation in the α subunit of transducin Yields a unique dominant-negative inhibitor. *J. Biol. Chem.* **280**, 35696–35703
36. Grishina, G., and Berlot, C. H. (1998) Mutations at the domain interface of Gsα Impair receptor-mediated activation by altering receptor and guanine nucleotide binding. *J. Biol. Chem.* **273**, 15053–15060
37. Tesmer, J. J. G., Sunahara, R. K., Gilman, A. G., and Sprang, S. R. (1997) Crystal structure of the Catalytic domains of adenylyl cyclase in a complex with Gsα-GTPγS. *Science* **278**, 1907–1916
38. Tesmer, V. M., Kawano, T., Shankaranarayanan, A., Kozasa, T., and Tesmer, J. J. G. (2005) Snapshot of activated G proteins at the membrane: the Gαq-GRK2-Gβγ; complex. *Science* **310**, 1686–1690
39. Lyon, A. M., Dutta, S., Boguth, C. A., Skiniotis, G., and Tesmer, J. J. G. (2013) Full-length Gαq–phospholipase C-β3 structure reveals interfaces of the C-terminal coiled-coil domain. *Nat. Struct. Mol. Biol.* **20**, 355–362
40. Chen, Z., Singer, W. D., Danesh, S. M., Sternweis, P. C., and Sprang, S. R. (2008) Recognition of the activated states of Galpha13 by the rgRGS domain of PDZRhoGEF. *Structure* **16**, 1532–1543
41. Hajicek, N., Kukimoto-Niino, M., Mishima-Tsumagari, C., Chow, C. R., Shirouzu, M., Terada, T., *et al.* (2011) Identification of critical residues in G(alpha)13 for stimulation of p115RhoGEF activity and the structure of the G(alpha)13-p115RhoGEF regulator of G protein signaling homology (RH) domain complex. *J. Biol. Chem.* **286**, 20625–20636
42. Slep, K. C., Kercher, M. A., He, W., Cowan, C. W., Wensel, T. G., and Sigler, P. B. (2001) Structural determinants for regulation of phosphodiesterase by a G protein at 2.0 Å. *Nature* **409**, 1071–1077
43. Chen, Z., Singer, W. D., Sternweis, P. C., and Sprang, S. R. (2005) Structure of the p115RhoGEF rgRGS domain–Gα13/i1 chimera complex suggests convergent evolution of a GTPase activator. *Nat. Struct. Mol. Biol.* **12**, 191–197
44. Day, P. W., Tesmer, J. J. G., Sterne-Marr, R., Freeman, L. C., Benovic, J. L., and Wedegaertner, P. B. (2004) Characterization of the GRK2 binding site of Galphaq. *J. Biol. Chem.* **279**, 53643–53652
45. Liu, W., and Northup, J. K. (1998) The helical domain of a G protein alpha subunit is a regulator of its effector. *Proc. Natl. Acad. Sci. U. S. A.* **95**, 12878–12883
46. Gao, Y., Eskici, G., Ramachandran, S., Poitevin, F., Seven, A. B., Panova, O., *et al.* (2020) Structure of the visual signaling complex between transducin and phosphodiesterase 6. *Mol. Cell* **80**, 237–245.e4
47. Kim, H. R., Ahn, D., Jo, J. B., and Chung, K. Y. (2022) Effect of α-helical domain of Gi/o α subunit on GDP/GTP turnover. *Biochem. J.* **479**, 1843–1855
48. Jones, J. C., Jones, A. M., Temple, B. R. S., and Dohlman, H. G. (2012) Differences in intradomain and interdomain motion confer distinct activation properties to structurally similar Gα proteins. *Proc. Natl. Acad. Sci. U. S. A.* **109**, 7275–7279
49. Marin, E. P., Krishna, A. G., Archambault, V., Simuni, E., Fu, W. Y., and Sakmar, T. P. (2001) The function of interdomain interactions in Controlling nucleotide exchange rates in transducin. *J. Biol. Chem.* **276**, 23873–23880
50. Toyama, Y., Kano, H., Mase, Y., Yokogawa, M., Osawa, M., and Shimada, I. (2017) Dynamic regulation of GDP binding to G proteins revealed by magnetic field-dependent NMR relaxation analyses. *Nat. Commun.* **8**, 14523
51. Noel, J. P., Hamm, H. E., and Sigler, P. B. (1993) The 2.2 Å crystal structure of transducin-α complexed with GTPγS. *Nature* **366**, 654–663
52. Codina, J., and Birnbaumer, L. (1994) Requirement for intramolecular domain interaction in activation of G protein alpha subunit by aluminum fluoride and GDP but not by GTP gamma S. *J. Biol. Chem.* **269**, 29339–29342
53. Marsh, S. R., Grishina, G., Wilson, P. T., and Berlot, C. H. (1998) Receptor-mediated activation of Gsα: evidence for intramolecular signal Transduction. *Mol. Pharmacol.* **53**, 981–990
54. Surve, C. R., To, J. Y., Malik, S., Kim, M., and Smrcka, A. V. (2016) Dynamic regulation of neutrophil polarity and migration by the heterotrimeric G protein subunits Galphai-GTP and Gbetagamma. *Sci. Signal.* **9**, ra22
55. Nobles, M., Montaigne, D., Sebastian, S., Birnbaumer, L., and Tinker, A. (2018) Differential effects of inhibitory G protein isoforms on G protein-gated inwardly rectifying K^+ currents in adult murine atria. *Am. J. Physiol. Cell Physiol.* **314**, C616–C626
56. Mumby, S. M., and Gilman, A. G. (1991) Synthetic peptide antisera with determined specificity for G protein alpha or beta subunits. *Methods Enzymol.* **195**, 215–233
57. McAlister, G. C., Nusinow, D. P., Jedrychowski, M. P., Wühr, M., Huttlin, E. L., Erickson, B. K., *et al.* (2014) MultiNotch MS3 enables accurate, Sensitive, and Multiplexed detection of differential expression across cancer cell line proteomes. *Anal. Chem.* **86**, 7150–7158
58. Mumby, S. M., and Linder, M. E. (1994) Myristoylation of G-protein alpha subunits. *Methods Enzymol.* **237**, 254–268
59. Dessauer, C. W. (2002) Kinetic analysis of the action of P-site analogs. *Methods Enzymol.* **345**, 112–126
60. Jo, S., Kim, T., Iyer, V. G., and Im, W. (2008) CHARMM-GUI: a web-based graphical user interface for CHARMM. *J. Comput. Chem.* **29**, 1859–1865
61. Hess, B., Kutzner, C., van der Spoel, D., and Lindahl, E. (2008) Gromacs 4: algorithms for highly efficient, Load-Balanced, and Scalable molecular simulation. *J. Chem. Theory Comput* **4**, 435–447
62. Huang, J., Rauscher, S., Nawrocki, G., Ran, T., Feig, M., de Groot, B. L., *et al.* (2017) CHARMM36m: an improved force field for folded and intrinsically disordered proteins. *Nat. Methods* **14**, 71–73
63. Berendsen, H. J. C., Postma, J. P. M., van Gunsteren, W. F., DiNola, A., and Haak, J. R. (1984) Molecular dynamics with coupling to an external bath. *J. Chem. Phys.* **81**, 3684–3690
64. Andersen, H. C. (1983) Rattle: a "velocity" version of the shake algorithm for molecular dynamics calculations. *J. Comput. Phys.* **52**, 24–34
65. Darden, T., Darrin, Y., and Pedersen, L. (1993) Particle mesh Ewald: an N ·log(N) method for Ewald sums in large systems. *J. Chem. Phys.* **98**, 10089–10092
66. Evans, D. J., and Holian, B. L. (1985) The Nose–Hoover thermostat. *J. Chem. Phys.* **83**, 4069–4074
67. Parrinello, M., and Rahman, A. (1981) Polymorphic transitions in single crystals: a new molecular dynamics method. *J. Appl. Phys.* **52**, 7182–7190
68. Petrova, S. S., and Solov'ev, A. D. (1997) The Origin of the method of steepest descent. *Hist. Math.* **24**, 361–375
69. Gogoshin, G. B., Boerwinkle, E., and Rodin, A. S. (2017) New algorithm and software (BNOmics) for Inferring and visualizing Bayesian networks from Heterogeneous Big biological and Genetic data. *J. Comput. Biol.* **24**, 340–356